Molecular Therapy
Methods & Clinical Development
Original Article

Optimization of hypo-alloimmunogenic multispecific CAR-T and SARS-CoV-2-specific T cells for off-the-shelf adoptive cell therapy

King Pan Ng,[1,3] Michaela Su-fern Seng,[1,2,3] and Wing Leung[1,2,3]

[1]Paediatric Bone Marrow Transplantation and Cell Therapy Centre, Children's Blood and Cancer Centre, KK Women's and Children's Hospital, SingHealth, Singapore, Singapore; [2]Department of Paediatric Haematology and Oncology, KK Women's and Children's Hospital, SingHealth, Singapore, Singapore; [3]Duke-NUS Medical School, Singapore, Singapore

Despite promising results with chimeric antigen receptor modified T(CAR-T) cells and virus-specific T(VST) cells, both forms of therapy are limited by timely availability, affordability, *in vivo* persistency, and antigen escape. To overcome these barriers, we developed multitargeting hypo-alloimmunogenic CAR-T and VST for off-the-shelf administration. We generated bi-specific CAR-T against CD19 and CD22 and tri-specific VST against S, M, and N proteins of SARS-CoV-2 for real patient use. Portions of these clinical-grade products were collected for proof-of-concept laboratory studies mimicking off-the-shelf settings. By electroporation delivery of Cas9 nuclease/guide RNA (gRNA) ribonucleoprotein, we developed a single-step approach to knockout B2M, achieving efficient (>80% of cells) B2M null on both bi-specific CAR-T and tri-specific VST, leading to marked reduction of allo-immunogenicity with intact potency, antigen specificity, phenotypes, and proliferative potential. Using newly designed paired Cas9 nickases-AAV6 B2M site-specific knockin system, we further refined the approach to re-express HLA-E in B2M null bi-specific CAR-T cells (>50% of cells), offering protection from natural killer cytotoxicity. The editing was highly specific with minimal off-target effects. Our approach enables expedient production of clinical-grade, off-the-shelf, hypo-alloimmunogenic, multi-specific CAR-T and VST, with improved potential for long-term *in vivo* persistence, primary disease control, genome-safety, immediate availability, product homogeneity, and reduced cost.

INTRODUCTION

Chimeric antigen receptor modified T (CAR-T) cells and virus-specific T (VST) cells are two common forms of cellular therapy. CAR-T are commercially available for B-lineage acute lymphoblastic leukemia, lymphoma, and myeloma,[1] whereas VST are available for Epstein-Barr virus (EBV) post-transplant lymphoproliferative disease.[2] Recently, VST have also been studied for the treatment of SARS-CoV-2 infections,[3–6] building a platform technology for future pandemics. Although the clinical results are promising, both CAR-T and VST have limitations in (1) timely availability, (2) affordability, (3) quality variability, and (4) *in vivo* persistency. Poor persistence of autologous CAR-T cells after infusion or even manufacturing failure are common, partly because these cells have often been exposed to intensive chemotherapy before collection for CAR-T manufacturing, whereas persistence of allogeneic CAR-T and VST is limited by allo-rejection.

To improve *in vivo* persistence, we developed herein proof-of-concept hypo-alloimmunogenic CAR-T and VST that could be administered off-the-shelf with optimized gene-editing efficiency, genome safety, and product affordability. Their efficacy was further enhanced by multitargeting, including bi-specific tandem CAR against both CD19 and CD22 tumor-associated antigens and tri-specific VST against the S, M, and N proteins of SARS-CoV-2.

RESULTS

Generation of multi-specific CAR-T and VST

A clinical trial for bi-specific CAR-T (NCT0542990) was conducted at our center, and five clinical products were generated under Good Manufacturing Practice (GMP) standards for autologous patient use. All five clinical bi-specific CAR-T products, which express anti-CD19-CAR and anti-CD22-CAR in tandem (Figure 1A), had high transduction efficiency, with an average of 69.3% CD3+ cells expressing CAR against CD19 and CD22 (Figure 1B; Table S1). Only trace amounts of natural killer (NK) cells were present, while all other immune cells were substantially depleted (including monocytes, B cells, neutrophils, and eosinophils) (Table S1). We examined the specific cytotoxicity of the bi-specific CAR-T using EuTDA assay. Raji ($CD19^+CD22^+$), RS4;11 ($CD19^+CD22^{dim}$), and K562 ($CD19^-CD22^-$) were chosen as target cells based on their antigen expression profiles. As expected, the CAR-T showed specific cytotoxicity toward target-positive Raji cells (average lysis of 32.2% at 10:1 effector to target ratio) and RS4;11 cells (21%), but with only minimal activity on the target-negative K562 cells (4.8%; Figure 1C).

Received 15 October 2024; accepted 4 April 2025;
https://doi.org/10.1016/j.omtm.2025.101462.

Correspondence: Wing Leung, Department of Paediatric Haematology and Oncology, KK Women's and Children's Hospital, Singapore, Singapore.
E-mail: leung.wing.hang@singhealth.com.sg

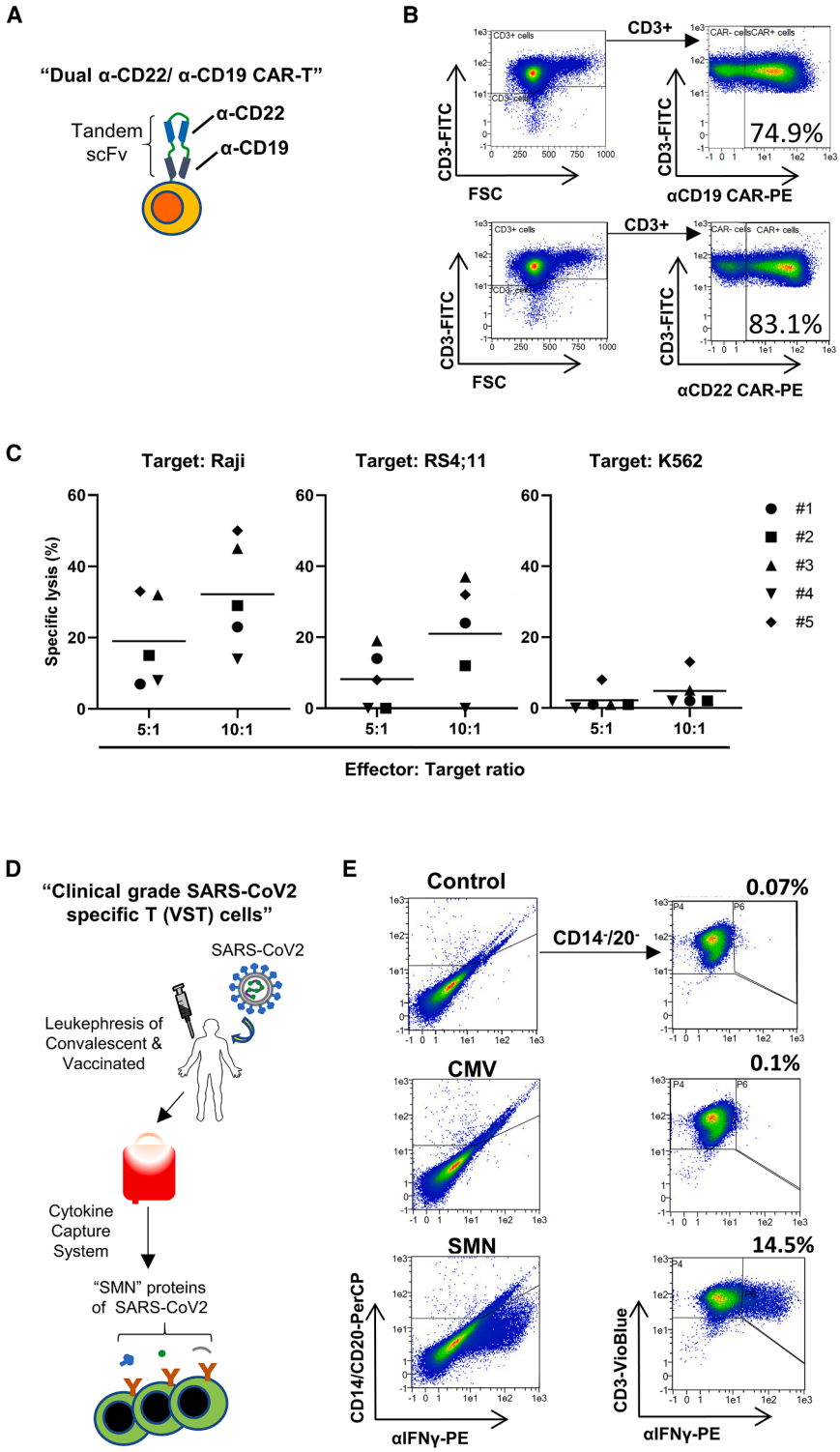

Figure 1. Generation of multispecific anti-CD22/ anti-CD19 CAR-T cells and anti-SMN SARS-CoV-2 T cells

(A) Illustration of the bi-specific CAR-T cells. ScFv; single chain fragment variable region. The CD19-CAR and CD22-CAR are expressed in tandem as a single molecule on the cell surface. (B) Characterization of bi-specific CAR-T product by flow cytometry. Representative flow plots showing cells stained for anti-CD19 CAR, anti-CD22 CAR, and CD3. (C) Specific cytotoxicity of the bi-specific CAR-T cells measured by EuTDA assay. The bi-specific CAR-T cells were incubated with the target cells at the effector: target ratio (E:T) of 5:1 and 10:1. The potency of bi-specific CAR-T cells are expressed as specific lysis (%) of target cells. (D) Illustration of SARS-CoV-2-specific T cells. Donors of SARS-CoV-2-specific T cells are either convalescent (n = 6), vaccinated (n = 1), or both (n = 1). One unit of whole blood or leukapheresis was collected from the donors, stimulated by the overlapping peptides pools of SARS-CoV-2 proteins S, M, and N. The functionally reactive, IFN-γ-expressing T cells were enriched by cytokine capture system (CCS, Miltenyi Biotec) and cryopreserved as clinical-grade products. (E) Specific reactivity to SMN peptide pool measured by intracellular IFN-γ assays. Flow plot of the intracellular IFN-γ assays (performed only on sample 8). The SARS-CoV-2-specific T cells were re-stimulated with no peptides (control), CMV, or SARS-CoV-2 peptides for 2 h and were incubated further for 4 more hours in the presence of brefeldin A. The cells were stained accordingly to the protocol of the rapid cytokines inspector kit, and IFN-γ expression in $CD3^+$ cells was quantified by flow cytometry. Figure reproduced from the prior publication[3] with new plots added.

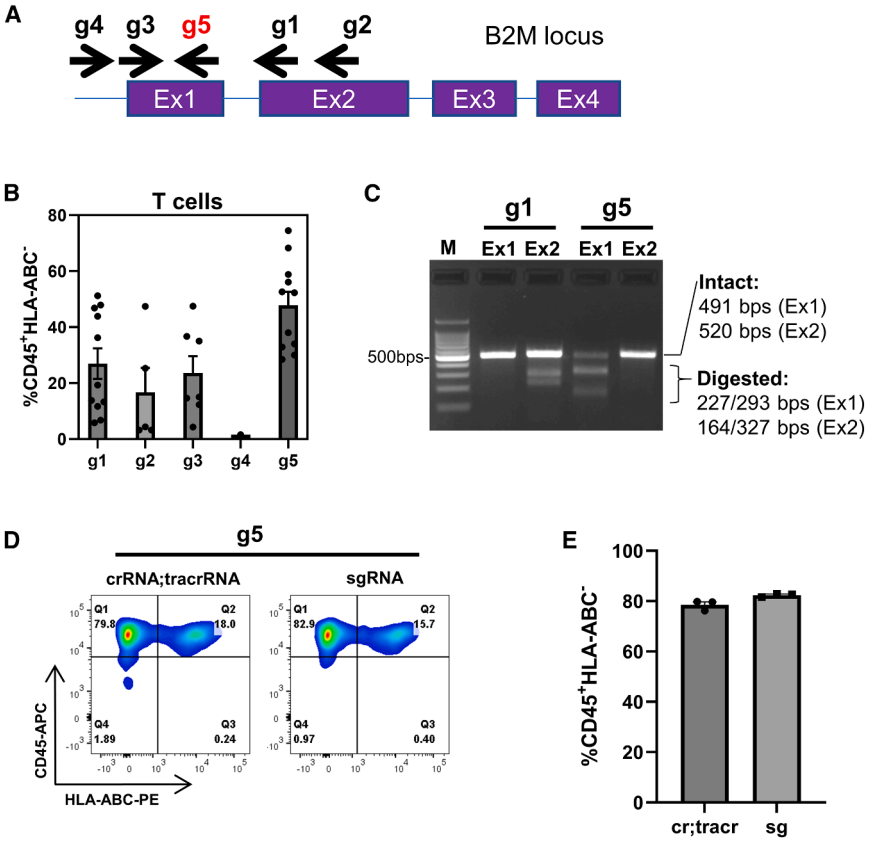

Figure 2. Optimization of B2M knockout by CRISPR-Cas9 ribonucleoprotein (RNP)

(A) Schematic of B2M locus on chromosome 15. The position and orientation of the candidate guide RNAs (gRNAs) are illustrated, with one gRNA targeting the promoter and two gRNAs each targeting exon 1 and exon 2, respectively. The best-performing gRNA g5 is highlighted in red and was used throughout the study. (B) Examining the gRNAs efficient. The gRNAs (crRNA; tracrRNA) were combined with Cas9 to generate the RNP complex, which was then electroporated into stimulated T cells. The cells were allowed to recover for 4 days in culture, and the percentage of HLA-ABC$^-$ cells was determined by flow cytometry using CD45 and HLA-ABC antibodies (n = 6–11). (C) Validation of genome editing. Genomic DNA was extracted from the cells 4 days post-electroporation and the region flanking the first exon of B2M gene was amplified for T7 endonuclease (T7E1) assay. The intact (~500 bps) and cleaved fragments (~200 and 300 bps) were resolved on 2% agarose gel. (D) Optimized editing using g5/Cas9 RNP complex. The g5, either in the form of crRNA;tracrRNA (cr) or single sgRNA (sg), was combined with Cas9-RNP for knockout of B2M in T cells, as described in (B). Representative flow plots show the level of HLA-ABC$^-$ cells. (E) The summary graph for experiment in (D) (n = 3).

In another set of trials (NCT04351659 and NCT04457726), we manufactured clinical-grade SARS-CoV-2-specific T cells under GMP standards from convalescent donors who had recovered from SARS-CoV-2 infection (henceforth referred to as VST) and the subsequently performed adoptive infusion of these VST to immunocompromised patients at risk of COVID-19 mortality. All clinical VST products (Figure 1D) were composed primarily of CD3$^+$ T cells (55% ± 4.7%, Table S2), with only trace amount of NK cells. To confirm their specificity in recognizing SARS-CoV-2 antigens, the interferon-γ (IFN-γ) response of one of the VST samples (8) was measured in the presence of peptides from specific antigens. Since the VST were produced by stimulation with overlapping peptides from the S, M, and N proteins of SARS-CoV-2 (the SMN peptides), these cells reacted only to the SMN peptides but not to those of cytomegalovirus (CMV) (Figure 1E) or EBV (data not shown).

Optimization of B2M knockout by CRISPR-Cas9 ribonucleoprotein (RNP)

To generate hypo-alloimmunogenic HLA-I null T cells, we designed five guide RNAs (gRNAs) targeting different parts of B2M gene (g1–g5; Figure 2A; Table S3). The gRNAs, in the form of crRNA;tracrRNA (Crispr RNA; trans-activating Crispr RNA) duplex, were combined with recombinant CRISPR-Cas9 nuclease to form ribonucleoprotein (RNP) complexes and delivered into activated normal T cells by electroporation. The g5, which targeted the first exon of B2M, showed the best efficiency in knocking out B2M and reducing HLA-ABC expression on the T cells (Figure 2B). The specificity of editing was confirmed by T7E1 endonuclease assay (mismatch cleavage assay), in which g5 specifically cleaved the PCR product amplified from the first but not the second exon of B2M (Figure 2C). For gRNA, a single gRNA molecule (sgRNA) is often considered more efficient than the crRNA; tracrRNA duplex[7]; however, we found that while using CRISPR-Cas9 RNP with optimization, both sgRNA and crRNA;tracrRNA worked equally well (Figures 2D and 2E). Thus, the crRNA;tracrRNA duplex was used for subsequent experiments to facilitate versatile multisite knockout (KO) when needed, allowing the use of various crRNA coupled with the universal tracrRNA.

Consistent KO of B2M in bi-specific CAR-T without affecting their CAR expression or proliferative potential

Next, we tested the B2M KO on the bi-specific CAR-T. Similar to normal T cells, g5 showed the best editing efficiency (Figures 3A and 3B); therefore, we went on to KO B2M on all five bi-specific CAR-T clinical products using g5. The KO was efficient generally, resulting in an average of ~80% of HLA-ABC$^-$ KO CAR-T cells in the samples (range from 68.4% to 88.3%; Figure 3C). Importantly, the B2M KO did not alter the proportion of CAR$^+$ cells in the KO samples in comparison to that of wildtype (WT) (mean 66.6% vs. 67.4%; Figure 3D). Within the KO samples, the proportion of CAR$^+$ cells were the same in the HLA-ABC$^+$ and HLA-ABC$^-$ subpopulations

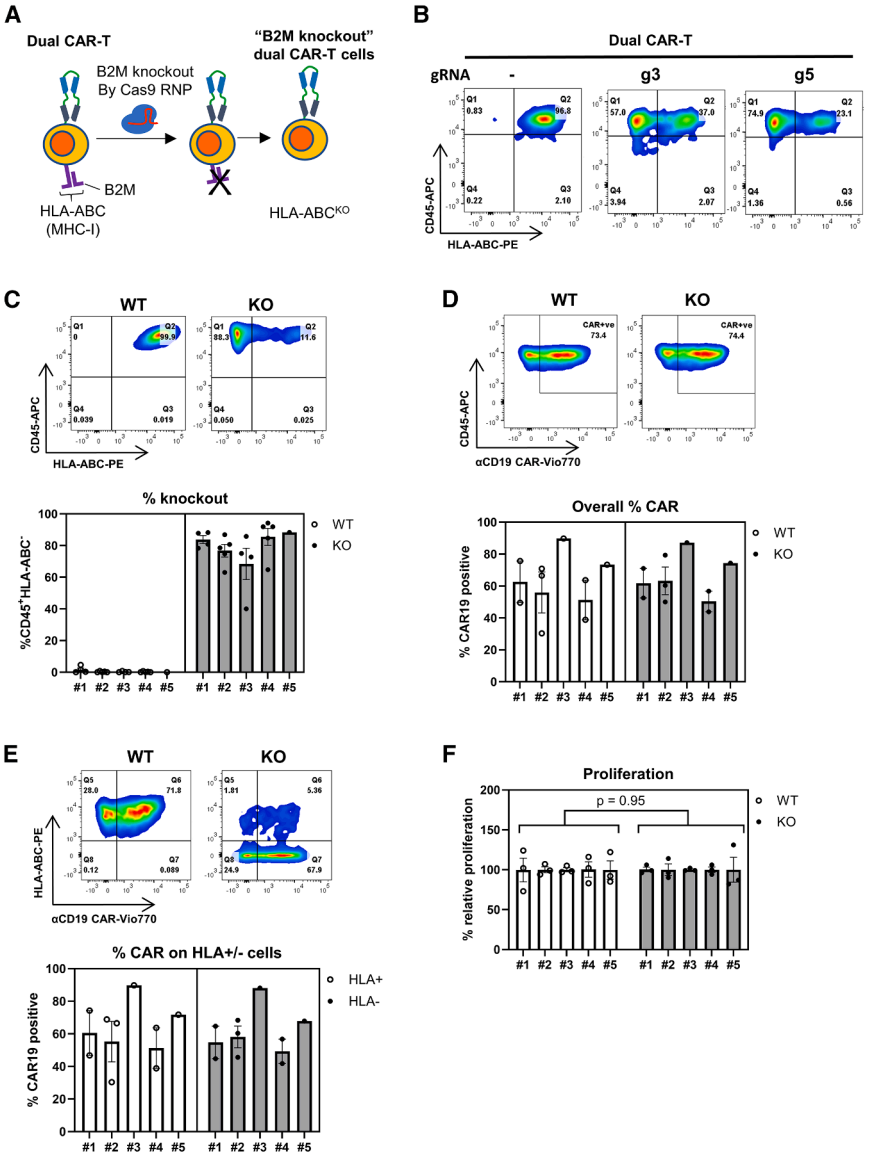

Figure 3. Consistent knockout of B2M in bi-specific CAR-T cells without affecting their CAR expression or proliferative potential

(A) Schematic of the study. B2M knockout abolishes the surface expression of all HLA class I (major histocompatibility complex class I) complexes (for simplicity, only HLA-A, HLA-B, and HLA-C are depicted), generating B2M null (i.e., HLA-I null), hypo-alloreactive bi-specific CAR-T cells for allogenic transfer.(B) Verification of B2M knockout in bi-specific CAR-T cells. The efficiency of promising gRNAs (g3 and g5) were examined on the bi-specific CAR-T cells. Representative flow plots are shown for bi-specific CAR-T sample 3.(C–E) Characterization of the edited bi-specific CAR-T cells. Showing the representative flow plots for sample 5 (top) and the summarized data for all five CAR-T samples (bottom). The levels of B2M knockout (CD45 and HLA-ABC), CAR-expressing cells (CD45 and CD19 CAR), and knockout of CAR-expressing cells (HLA-ABC and CD19 CAR staining) are shown in (C), (D), and (E), respectively (n = 3–5 for each samples). (F) Proliferation of the edited bi-specific CAR-T cells. Five days post electroporation, the cells were plated and incubated further for an additional 5 days, after which proliferation was assessed using DELFIA assay. The rate of proliferation of wild-type cells was set at 100%, and triplicates were performed for each sample.

(mean CAR$^+$/HLA$^+$ vs. CAR$^+$/HLA$^-$, 65.7% vs. 63.6%; Figure 3E), confirming that the presence of CAR did not interfere with B2M KO mediated by CRISPR-Cas9; in turn, B2M KO did not affect CAR-expression. Furthermore, as measured by the DELFIA cell proliferation assay, B2M KO did not alter the proliferative potential of CAR-T (Figure 3F).

B2M null bi-specific CAR-T were hypo-alloimmunogenic but retained antileukemic potency

To confirm the reduction in alloimmunogenicity of the B2M KO CAR-T, we performed a one-way mixed leukocyte reaction (MLR) assay (Figure 4A). In the assay, the bi-specific CAR-T (as stimulators) and third-party donor cells (as responders) were labeled with Violet and CFSE, respectively. The stimulators were growth-arrested by irradiation before being co-cultured with the responders. By the end of the 6–7 day co-culture, the percentage of highly proliferative responder T cells (CD3$^+$/CFSE^{dim}; violet$^-$), which correlated with the alloimmunogenicity of stimulators, was determined by flow cytometry. In MLR assays using normal T responder cells (untransduced, non-CAR) and B2M-null stimulator population purified (>98%) by magnetic bead separation, the purified KO cells markedly reduced the number of CD3$^+$/CFSE^{dim} responder T cells (WT, 12.5%; KO, 1.7%; i.e., KO was 13.6% of the WT) (Figure 4B, top). For bi-specific CAR-T stimulator, even without depleting the residual bi-specific HLA-ABC$^+$ cells (percentage of HLA-ABC$^-$ CAR-T in samples 1 to 5: 80%, 80%, 73%, 65%, and 88%, respectively), B2M KO still significantly reduced the percentage of CD3$^+$/CFSE^{dim} responder T cells (36 ± 14.9% of the WT; Figure 4C), demonstrating diminished alloimmunogenicity.

At effector to target (E:T) ratio of 10:1, the average specific lysis on Raji, RS4;11, and K562 by the bi-specific CAR-T before B2M KO was 43%, 40%, and 11%, respectively. In comparison, the B2M KO bi-specific CAR-T possessed similar level of specific cytotoxicity (average specific lysis of Raji, RS4;11, and K562 was 42%, 40%, and 11%, respectively) (Figure 4D). Collectively, the results demonstrate that our editing approach successfully generates hypo-alloimmunogenic bi-specific CAR-T cells without compromising antileukemic potency.

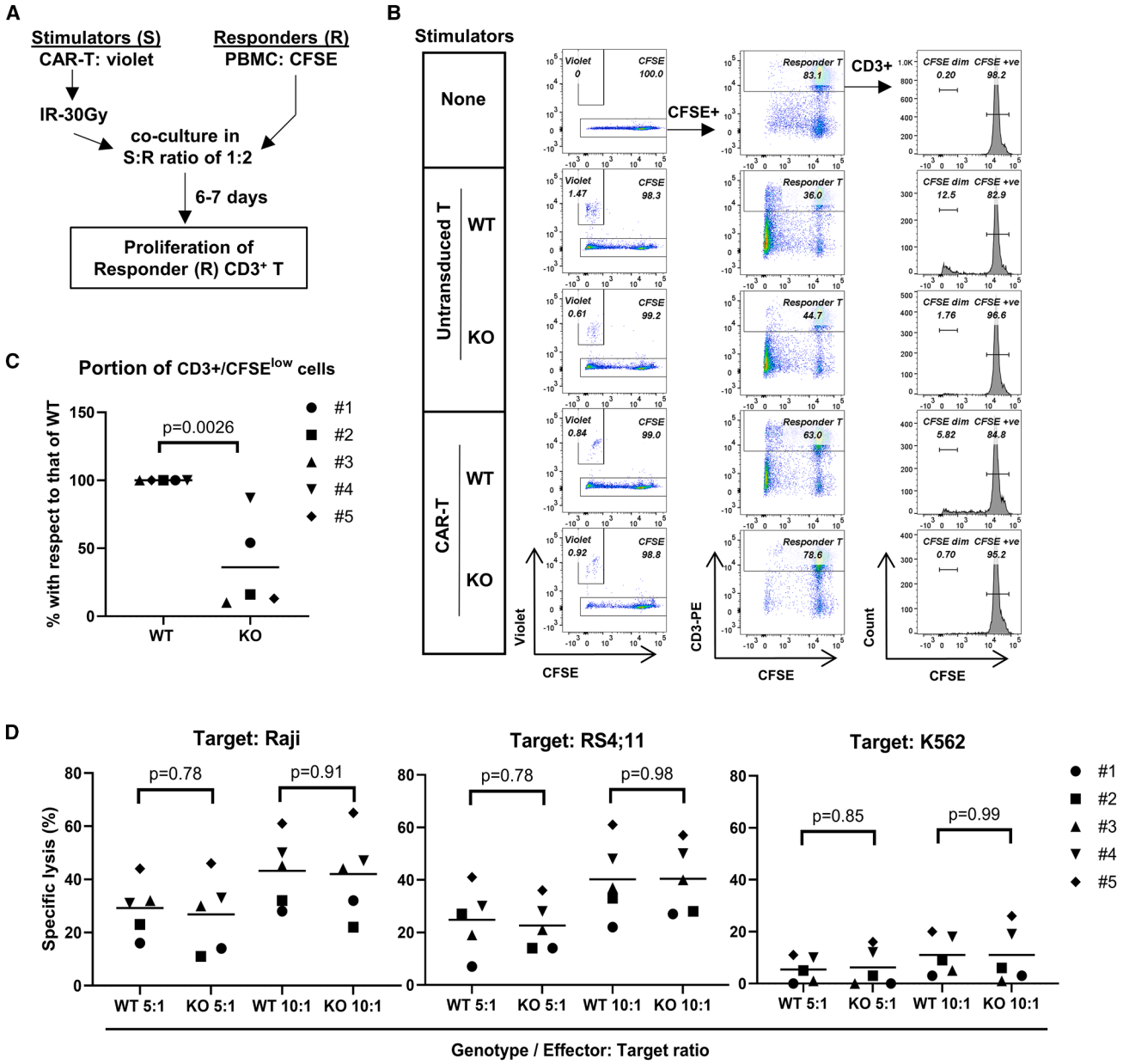

Figure 4. B2M dull bi-specific CAR-T cells were hypo-alloimmunogenic but retained antileukemic potency

(A) Schematic of the mixed leukocyte reaction (MLR) assay. The irradiated stimulators (bi-specific CAR-T cells or normal T cells) and the responder cells (allogenic PBMC; peripheral blood mononuclear cells) were fluorescent labeled by Celltrace Violet and CFSE, respectively, and co-cultured at a stimulators to responder (S:R) ratio of 1:2 for 6–7 days. The proliferation of allogenic responder T cells was then analyzed by flow cytometry. (B) Representative flow plots showing the gating strategy for MLR (bi-specific CAR-T sample 3). A set of no stimulator cells (none), wild-type, and knockout normal T cells (untransduced, non-CAR) were included for validation. The irradiated, non-proliferative bi-specific CAR-T cells (violet^{+}) were distinguished from the allogenic responder cells (CFSE$^{+/-}$; proliferating cells exhibited diminished CFSE signal). The percentage of highly proliferative responder T cells (CD3^{+}CFSE^{dim}) within the total CD3^{+}CFSE^{+} cells was determined using histogram for each sample. (C) Summary graph showing the proportion of highly proliferative responder T cells (CD3^{+}CFSE^{dim}) in (B) for each individual sample, with the level of wild-type stimulator cells set at 100%. The percentages of B2M null cells in the knockout samples 1–5 were 80%, 80%, 73%, 65%, and 88%, respectively. (D) Specific cytotoxicity of the edited bi-specific CAR-T cells measured by EuTDA assay. The bi-specific CAR-T cells were incubated with the target cells at the effector: target ratio (E:T) of 5:1 and 10:1, with the potency expressed as specific lysis (%) of the target cells (n = 5, one experiment for each sample).

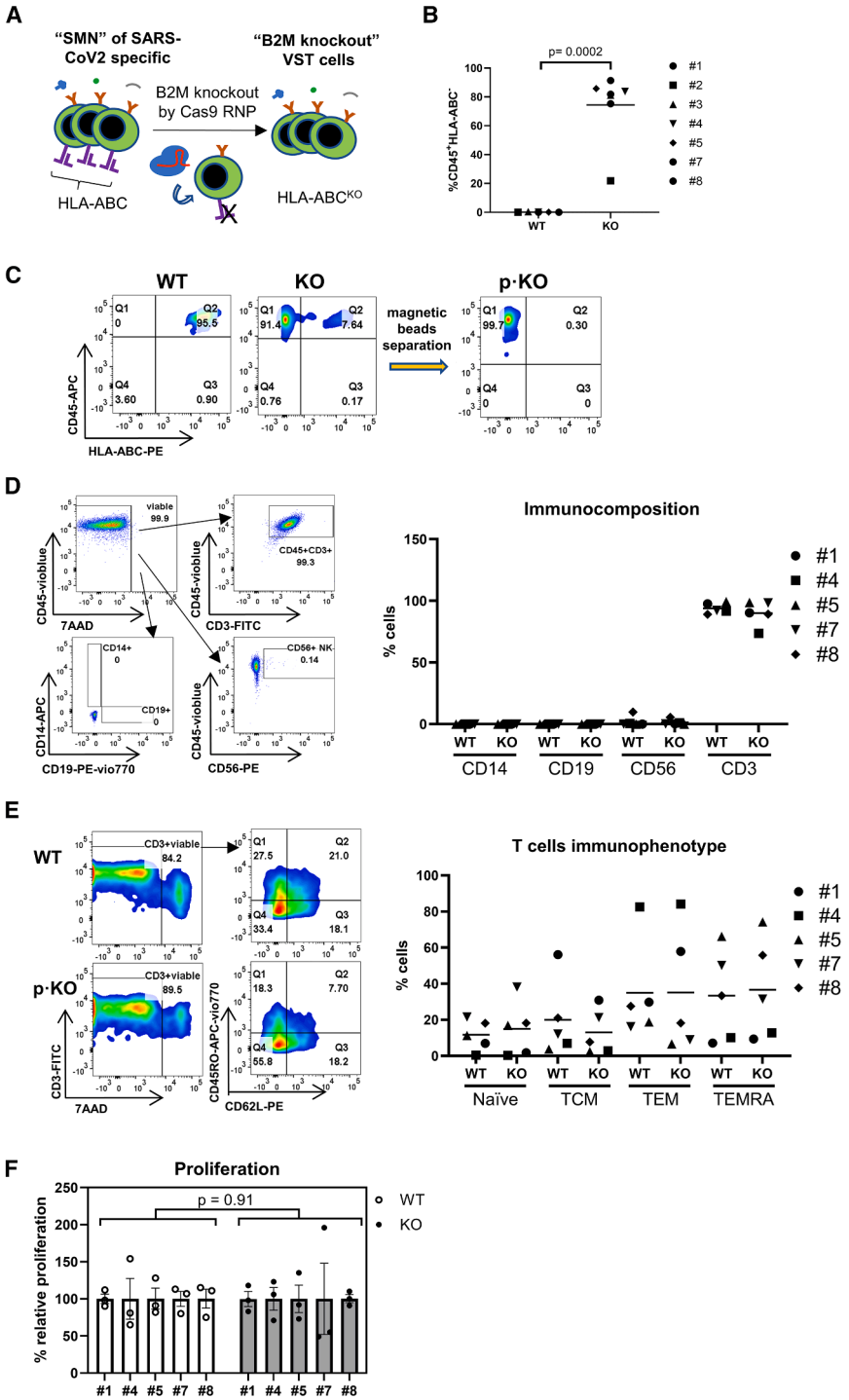

Figure 5. Consistent knockout of B2M in SARS-CoV-2-specific T cells without affecting their memory-cell phenotype or proliferative potential

(A) Schematic overview of the generation of the B2M knockout SARS-CoV-2-specific T cells. (B) Efficiency of B2M knockout on SARS-CoV-2-specific T cells. The SARS-CoV-2-specific T cells was expanded and electroporated with Cas9-RNP. The percentage of HLA-ABC$^-$ cells was determined by flow cytometry 4 days later, and the summarized graph are shown (n = 7, one experiment per sample). (C) The B2M knockout cells were further enriched by cell-depletion using HLA-ABC-biotin-streptavidin microbeads and magnetic beads column, at which the enrichment was >98% for all samples (p·KO; pure knockout). Representative flow plots shown for one sample (7). (D) Immunocomposition and the representative flow plots showing the gating strategy (sample 3). The cells were gated for CD45$^+$, and then gated separately for CD14$^+$, CD19$^+$, CD56$^+$, and CD3$^+$. The summary graph for all samples is shown on the right. (E) Immunophenotype of the SARS-CoV-2-specific T cells and the representative flow plots (sample 8). The viable CD3$^+$ cells were gated for CD62L$^+$/CD45RO$^+$ subpopulations. The summary graph for all sample is shown on the right. Naive, CD62L$^+$ CD45RO$^-$ naive T cells; TCM, CD62L$^+$CD45RO$^+$ T central memory cells; TEM, CD62L$^-$CD45RO$^+$ T effector memory cells; TEMRA, CD62L$^-$CD45RO$^-$ T terminal effector memory RA$^+$ cells. (F) Proliferation of the edited SARS-CoV-2-specific T cells. Five days post electroporation, the cells were plated and incubated for another 5 days, before being subjected to DELFIA assay. The proliferation rate of wild-type cells set at 100%, and triplicates were performed for each sample.

Consistent knockout of B2M in SARS-CoV-2 VST without affecting their memory-cell phenotype or proliferative potential

Reducing alloimmunogenicity could improve *in vivo* persistency of other cell therapies such as allogeneic VST. Particularly in a pandemic situation, the generation of large amount of VST suitable for large numbers of recipients is crucial. As a proof of concept, we examined the feasibility of our B2M editing approach on the anti-SMN SARS-CoV-2-specific T cells that were generated for adoptive transfer to immunocompromised patients (NCT04351659 and NCT04457726).[3,6] These cells were harvested from convalescent and/or vaccinated individuals and cryopreserved (Figure 5A). For the majority of these clinical products, we successfully thawed, expanded and gene-edited the tri-specific anti-SMN VST, except for one (2) which was not expanding well after thaw and electroporation (Figure 5B; Table S2). Similar to what we observed on CAR-T, approximately 80% B2M KO was achieved in the VST (Figure 5B).

By magnetic bead separation, we produced a highly purified KO population (p·KO, >98% of HLA-ABC$^-$ cells; Figure 5C). Compared

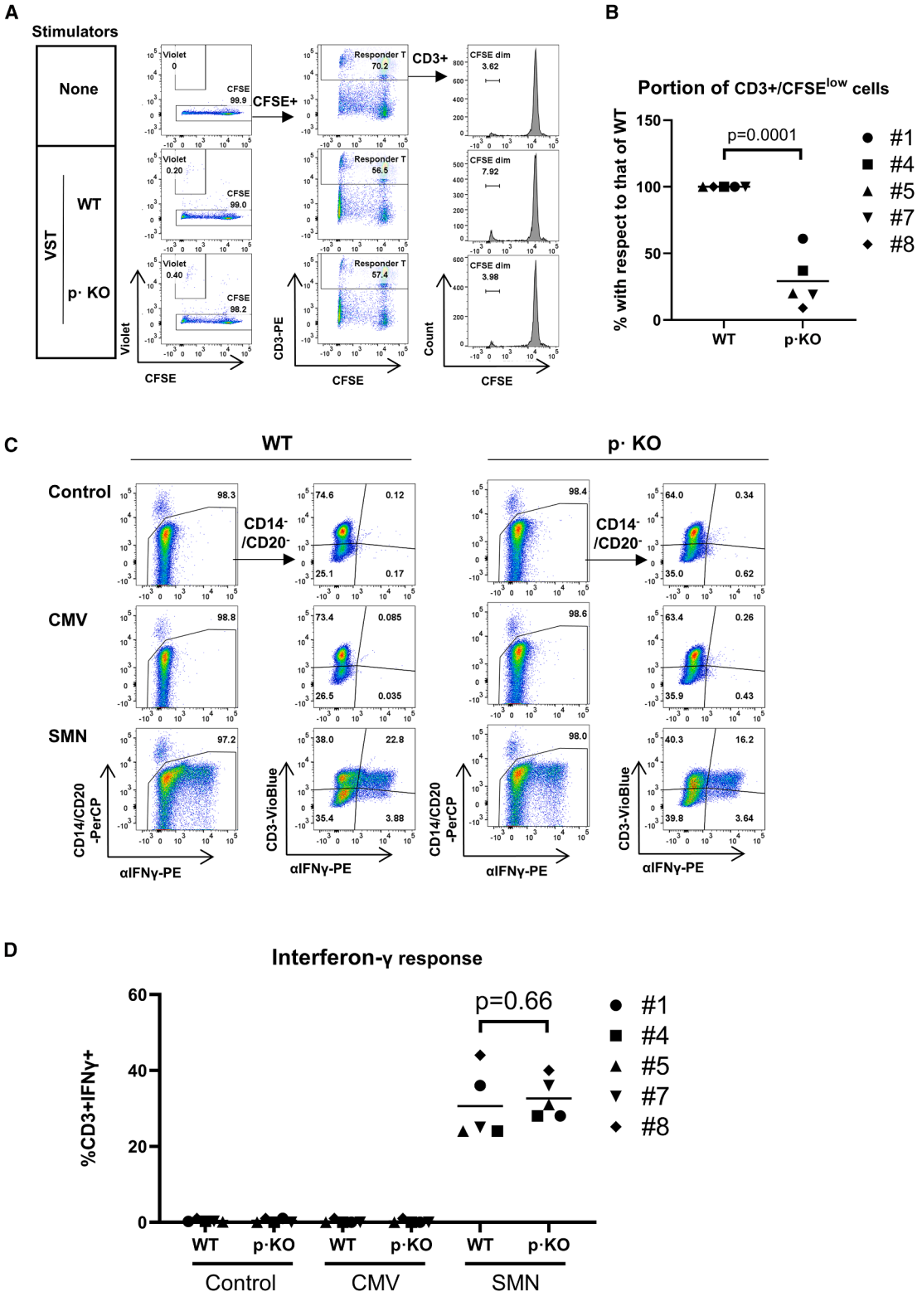

(legend on next page)

with the original clinical products, the expanded VST cells (both WT and p·KO) were free of monocytes and B cells (Figure 5D; Table S4) and enriched in T cells with the following composition: T effector memory cells (TEM) ($CD62L^{-}CD45RO^{+}$; 35.1% ± 9.22), terminal effector memory $CD45RA^{+}$ cells (TEMRA) ($CD62L^{-}CD45RO^{-}$; 35.1% ± 7.98), T central memory cells (TCM) ($CD62L^{+}CD45RO^{+}$; 16.5% + 5.33), and naive T cells ($CD62L^{+}CD45RO^{-}$; 13.4% ± 3.74) (Figure 5E; Table S4). Importantly, the KO of B2M did not alter the composition of memory cell phenotypes and did not dampen their proliferative potential (Figure 5F).

B2M knockout SARS-CoV-2 VST were hypo-alloimmunogenic but retained anti-SMN potency

B2M KO of the SARS-CoV-2 VST significantly reduced their alloimmunogenicity in MLR assay (average 29.1% of the WT, Figures 6A and 6B). To confirm the specificity and potency of the B2M KO VST, we measured their IFN-γ response to specific SARS-CoV-2 SMN peptides. As expected, VST reacted only to the SMN peptides but not to those of CMV (Figure 6C) or EBV (data not shown). There was no notable difference in the extent of IFN-γ response between the WT and p·KO cells when challenged with the SMN peptides (Figure 6D), implying that the edited VST retained their functionality and specificity in recognizing SARS-CoV-2 antigens. Taken together, these observations demonstrated the generalizability of our B2M editing approach to both clinical-grade CAR-T and VST.

Analysis on editing specificity of B2M knockout

While the on-target editing of B2M is efficient, CRISPR-Cas9 nuclease might introduce unwanted, off-target mutations that could potentially pose safety concern for clinical use. To provide insight for the specificity of g5, we employed targeted amplicon sequencing to analyze the editing profile of the B2M KO samples, for both bi-specific CAR-T (KO, 1–5) and tri-specific VST (KO, 2 and 3; p·KO for 1, 4, and 5). The amplicon panel comprised the B2M site (On-1) as well as 13 potential off-target sites (Off_1–Off_13) sharing high homology with the guide sequence of g5 (Figure S1A). The pair-end sequencing data were reassembled, merged, and fully mapped to the target sites (Tables S5 and S6 for CAR-T and VST, respectively), with all types of genomic variations categorized (Tables S7 and S8 for CAR-T and VST, respectively). The percentage of non-homologous end-joining, which represented the insertions and deletions (indels) generated exclusively by CRISPR-Cas9 editing, was summarized in Figure S1B. Expectedly the on-target editing was very efficient, with indels exceeding 96% on the KO samples of the bi-specific CAR-T, resulting in ∼80% frameshift, which was largely consistent with the percentage of $HLA\text{-}ABC^{-}$ cells observed via flow cytometry. The editing was equally efficient on VST, with the percentage of indels being significantly higher in p·KO samples (>98%) than in KO (60%–65%). For off-target effects, only two KO samples showed a slightly higher level of indels (0.5% and 0.8%) on one of the off-target sites (Off_1 on chromosome 17, which had no nearby gene), while at all other off-target sites, the levels of indels are similar between KO and the respective WT samples (Figure S1B; Tables S9 and S10 for CAR-T and VST respectively). Interestingly, the indel profiles on the B2M site were similar across the KO samples (Figure S1C; representative profiles of p·KO samples), demonstrating the high specificity and reproducibility of the Cas9 RNPs editing approach, with negligible off-target mutations.

Strategy to express B2M-HLA-E fusion by site-specific knockin to the B2M loci

While KO of B2M reduces T cell alloimmunogenicity, the complete depletion of HLA class I molecules may elicit lysis by NK cells, which could be counteracted by re-expressing the minimally polymorphic HLA-E, which binds the inhibitory receptors NKG2A/B on the NK cells.[8,9] When fused to B2M, the HLA-E molecules could be re-expressed on the cell surface specifically, even without endogenous B2M.[8,10] We tested if this was feasible to knock in a B2M-fused HLA-E expression cassette exactly at the B2M locus targeted by g5 through homologous direct repair (HDR) (Figure 7A). The DNA repair template, which contains an upstream homologous arm (HA) (5′HA; 800 bps specific to the B2M promoter and part of first exon, upstream of the g5 target site), the expression cassette for B2M-flexible linker (G4S)-HLA-E (B2M-HLA-E) fusion, and a downstream HA (3′HA; 800 bps specific to the first intron of B2M downstream of the gRNA target site), was delivered to the cells by adeno-associated virus (AAV serotype 6, which is specific for T cells). Another AAV repair template expressing EGFP was constructed as reporter (sequences of the templates can be found in Table S11). While Cas9-mediated DNA breakage could be used to initiate HDR, we hypothesized that its efficiency could be enhanced by Cas9 nickase (Cas9n), which produces a single-strand DNA nick (break) instead. When Cas9n is complexed with two gRNAs targeting opposite DNA strand in a close proximity (tens to hundreds of base pairs apart) and with the protospacer-adjacent motif (PAM) of each gRNA facing outward from the target region (the PAM-out configuration), the two DNA nicks create a double strands DNA break with 5′ overhangs, in contrast to the blunt-end break created by Cas9.[11] These 5′ overhangs facilitate HDR, leading to efficient knockin in the presence of a DNA repair template.[12,13]

Paired Cas9 nickase allows efficient knockin and eliminates off-target editing

Given the aforementioned rationale, we searched for additional gRNAs that could pair with g5 in a PAM-out configuration for creating break at B2M locus. We identified 3 gRNAs (s1, s2, and

Figure 6. B2M knockdown SARS-CoV-2 T cells were hypo-alloimmunogenic but retained anti-SMN potency

(A) MLR assay for the edited SARS-CoV-2-specific T cells. Experimental set up and analysis were the same as described before (Figures 4A and 4B), except that SARS-CoV-2-specific T cells were used as stimulator. (B) Summary graph showing the proportion of highly proliferative responder T cells ($CD3^{+}CFSE^{dim}$) in (A) for individual sample, with the level of wild-type stimulator cells set as 100%. (C and D) Intracellular interferon-γ (IFN-γ) assays. Experimental setup was described before (Figure 1E). Representative flow plots for sample 1 are shown, and the summary graph is presented in (D).

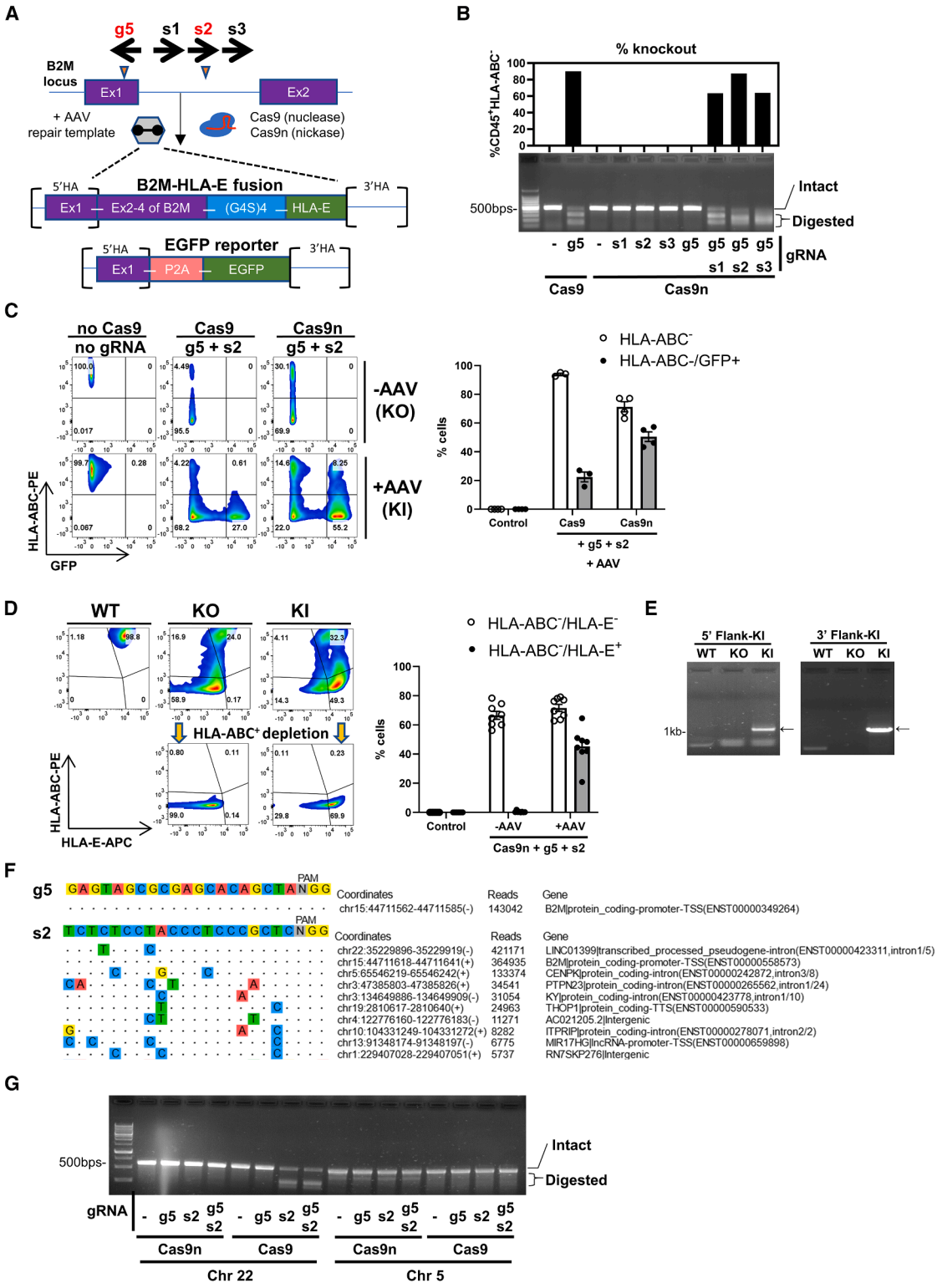

Figure 7. Knock in of B2M-HLA-E fusion to the B2M gene locus

(A) Schematic representation of the strategy to re-express B2M-HLA-E fusion in B2M knockout cells. Paired gRNAs (g5 and s1-3) were complexed with Cas9 nuclease (Cas9) or nickase (cas9n) to mediate B2M knockout and the knockin of B2M-HLA-E (or EGFP, as reporter) in the presence of single-strand DNA repair template delivered by

(legend continued on next page)

s3; Figures 7A and S2A) that share similar 3′HA and could potentially pair with g5 and Cas9n. We first examined the efficiency of these gRNAs on B2M KO in normal T cells. As expected, none of these gRNAs alone could produce editing in combination with Cas9n; editing was observed only when a pair of gRNAs was used, with the g5-s2 pair being most efficient (Figure 7B). We then tested whether Cas9n could outperform Cas9 for HDR using the EGFP repair template, which carried 3′HA compatible to site targeted by s2. As an expression vector, the AAV template did not integrate to the genome and did not express at high levels (Figure 7C). The AAV template only integrated in the presence of g5-s2 RNP of Cas9 or Cas9n. Remarkably, Cas9n is much more efficient in creating a knockin, producing ∼50% of GFP^+/$HLA\text{-}ABC^-$ cells (50.5 ± 3.4%, versus 22.5 ± 3.5 by Cas9; Figure 7C). The AAV integration is specific to the B2M locus, as strong GFP expression was observed only in cells edited with g5 or s2 but not by control gRNA targeting elsewhere (Figure S2B). The GFP^+/$HLA\text{-}ABC^-$ (knockin) cells consisted of a GFP^{high} and a GFP^{low} populations (signal on a log scale; Figures S2B and S2C) with the intensity of GFP signals roughly in a 2:1 ratio, respectively. Additionally, there was a small population of GFP^+/$HLA\text{-}ABC^+$ cells. We reasoned that these could be attributed to allelic KO/knockin, at which the GFP^{high} and GFP^{low} populations (of GFP^+/$HLA\text{-}ABC^-$) represent the cells having genotype of $B2M^{KI/KI}$ (two copies of GFP) and $B2M^{KI/KO}$ (one copy of GFP), respectively, while the GFP^+/$HLA\text{-}ABC^+$ cells represent genotype of $B2M^{KI/WT}$ (Figure S2C). After establishing the Cas9n;g5-s2 pair, we deployed it to create B2M-HLA-E knockin cells (KI) using the AAV template. Similarly, the Cas9n;g5-s2 RNP efficiently produced $HLA\text{-}ABC^-$/$HLA\text{-}E^+$ cells having surface expression of HLA-E readily detected by flow cytometry (of the KI, 45.3 ± 4.3%; Figure 7D). We further depleted the unedited cells in both KO and KI in one sample to verify the expression of HLA-ABC and HLA-E of the edited cells by flow cytometry (Figure 7D). We confirmed the integration of the B2M-HLA-E cassette by PCR amplification of regions flanking the 5′HA and 3′HA to the coding region of B2M-HLA-E (Figure 7E). Taken together, the Cas9n-AAV6 knockin approach worked well in producing the B2M null, HLE-E expressing T cells.

Lastly, to gain insight to the specificity of g5-s2 pair, we employed genome-wide, unbiased identification of DSBs enabled by sequencing (GUIDE-seq) to identify potential off-target sites of the two gRNAs in combined with Cas9 nuclease.[14,15] The g5 is highly specific, with only on-target editing to the intended B2M locus (Figure 7F; Tables S12 and S13), consistent with the analysis of targeted amplicon sequencing (Figure S1B). In comparison, s2 is less specific, with two main off-target sites identified on chromosome 22 (chr22; chr22:35229896-35229919) and chromosome 5 (chr5; chr5:65546219-65546242) (Figure 7F; Table S14). We tried to verify these potential off-target sites by T7E1 assay. We detected substantial editing at the chr22 site on cells edited with Cas9;s2 or Cas9;g5-s2 (Figures 7G and S2D). In sharp contrast, this off-target editing was completely absent in cells edited with Cas9n instead of Cas9 nuclease. No trace of editing was found on the chr5 site (Figures 7G and S2D). In summary, our result demonstrated the "paired nickase" strategy enables efficient and site-specific knock in while eliminating potential off-target editing mediated by Cas9 nuclease.

B2M-HLA-E fusion cf. resistance to cytotoxicity induced by NK cells

Next, we examined whether the B2M-HLA-E could functionally suppress NK-cell activity using the well-established NK92MI cell model. The edited T cells were co-cultured with NK92MI cells for 3 days, and the composition of remaining T cells in the culture was analyzed by flow cytometry (Figure 8A). Co-culture with NK92MI markedly reduced the proportion of total $HLA\text{-}ABC^-$ cells in the KO, which could be prevented by the knock in among KI T cells (29.3% ± 2% and 68.1 ± 6.3%, percentage of $HLA\text{-}ABC^-$ cells among KO versus KI; Figure 8B), suggesting specific depletion of $HLA\text{-}ABC^-$ cells by NK92MI in the absence of HLA-E.

We thus moved on to ask if the knock in could confer protection from primary NK cells as well. Primary NK cells were isolated from healthy donors, and the expression of receptors NKG2A and NKG2C was analyzed by flow cytometry (Figure 8C). Similar to NK92MI, nine out of ten NK samples predominantly expressed

AAV (serotype 6). AAV: adeno-associated virus; (G4S)4: flexible linker contains 4× Gly-Gly-Gly-Gly-Ser; P2A: 2A peptides facilitating ribosomal skipping during translation; HA: homologous arm. The most efficient gRNA pair g5 and s2 (highlighted red) was chosen for further experiments. (B) Evaluation of editing efficiency of g5 and s1-3 at B2M gene. The gRNAs were combined with Cas9 or Cas9n to generate the RNP complex, which was delivered to normal T cells as previously described. Four days post-electroporation, the cells were harvested to determine the percentage of $HLA\text{-}ABC^-$ cells by flow cytometry (top) or to estimate the efficiency of editing by the same T7E1 assay for B2M (bottom). (C) Assessment of knockin efficiency at B2M locus using the EGFP expression cassette. The experiment set up was the same as in (B), except that AAV particles were either included or omitted post-electroporation. Four days later, the cells were analyzed by flow cytometry for HLA-ABC and EGFP expression. The representative flow and the summary graph of results is shown on the right (n = 3). (D) Knockin of B2M-HLA-E fusion in normal T cells. The experimental setup was the same as in (C) except the AAV particles containing cassette expressing B2M-HLA-E were used. HLA-ABC and HLA-E expression was determined by flow cytometry, with representative flow plots shown. $HLA\text{-}ABC^+$ cells were depleted in one sample to obtain the purified knockout (KO) and knockin (KI) cells. The summary graph of knockin experiment is shown on the right (n = 8). (E) Verification of knockin at the genome level. Genomic DNA were isolated from edited cells. PCR products (highlighted by arrows) were amplified using primers specific to the 5′ or 3′ of the B2M-HLA-E fusion expression cassette and the flanking region of the targeted B2M locus. PCR products were resolved on a 1% agarose gel. (F) GUIDE-seq analysis for g5 and s2. The on-target and potential off-target editing sites were summarized. Each row represented one site, detailing its nucleotide sequence, annotated coordinates, the GUIDE-seq read counts, and a brief description. Off-target site mismatches were highlighted using colored nucleotides. (G) Evaluation of potential off-target sites for gRNA s2. The same T7E1 assay was performed on gDNA extracted from T cells edited using g5 and/or s2, combined with either wild-type Cas9 or Cas9n. Primers specific for the two most prominent off-target sites (chr22 and chr5; identified in (F)) were used. The digested PCR products were resolved on a 2% agarose gel.

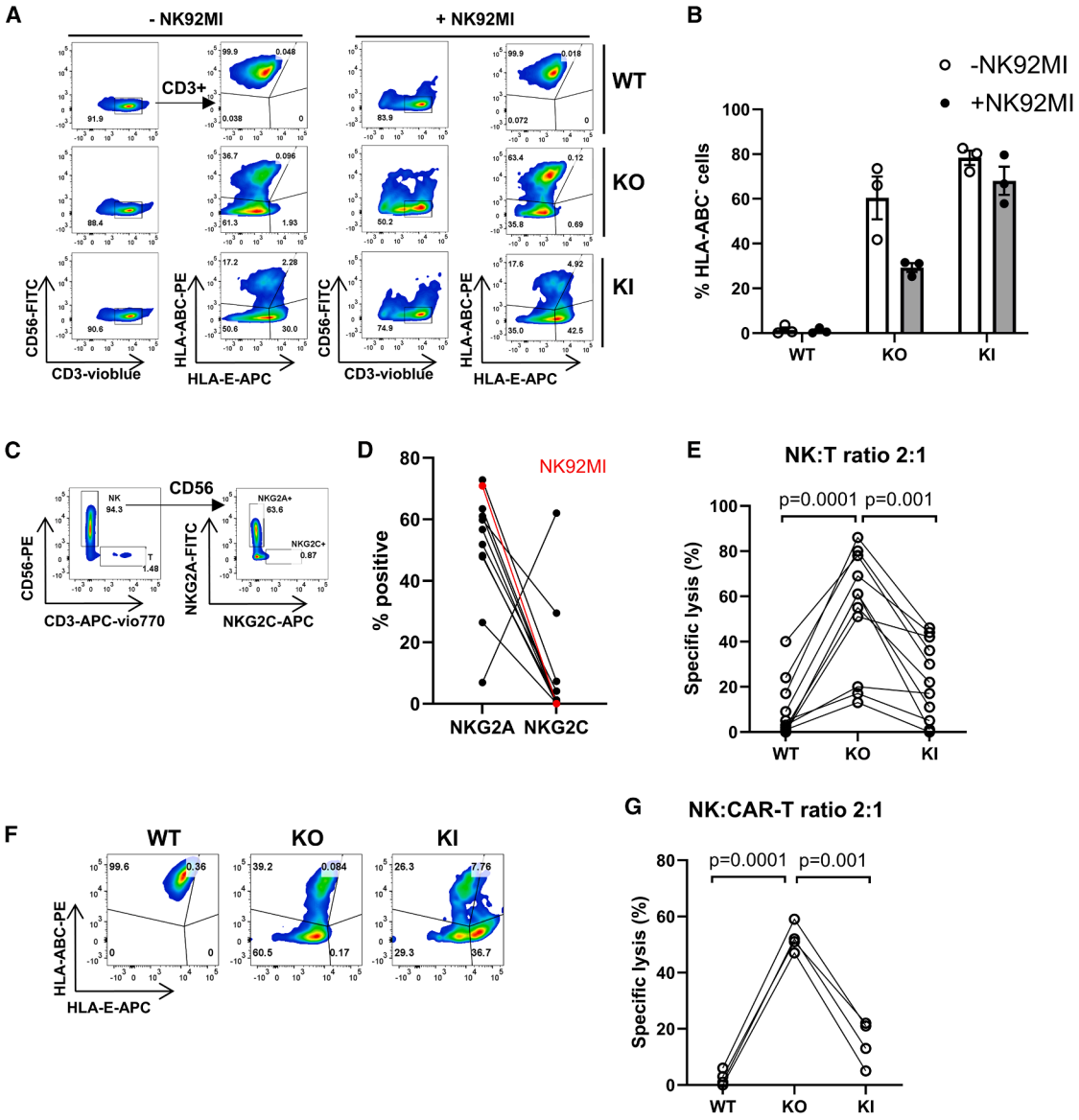

Figure 8. Suppressing activity of NK cells by B2M-HLA-E fusion

(A) Co-culture of edited T cells with NK92MI cells. Edited T cells were co-cultured with NK92MI for three days before being harvested for flow cytometry. T cells were gated by $CD56^{-}CD3^{+}$, and their HLA-ABC and HLA-E expression was analyzed by flow cytometry. The summary graph showing the percentage of $HLA\text{-}ABC^{-}$ cells I presented is shown in (B) ($n = 3$). (C) Analysis of primary NK cells. The percentage of $CD56^{+}$ NK cells expressing receptors NKG2A and/or NKG2C were quantified by flow cytometry. The summary graph, including data from NK92MI (highlight in red) and 10 primary NK cell samples, is shown in (D) ($n = 10$). (E) Specific cytotoxicity of primary NK cells against edited T cells was measured by EuTDA assay. NK cells (effector, E) and edited T cells (targets, T) were co-cultured at the E:T ratio of 2:1 for 3 h before determining specific lysis of T cells. Summarized data showing 11 experimental sets from five T cell samples in combinations with seven allogenic NK cell samples (all expressing NKG2A at significantly higher levels than NKG2C). (F) Knock in of B2M-HLA-E in bi-specific CAR-T sample. The same analysis as described in Figure 7D was performed. (G) Specific cytotoxicity of primary NK cells against edited bi-specific CAR-T cells was measured by EuTDA assay. Primary NK cells and edited bi-specific CAR-T cells were co-cultured at E:T ratio of 2:1 for 3–4 h, after which specific lysis of T cells was determined ($n = 4$).

NKG2A (Figure 8D), consistent with prior studies.[10,16] We then examined the cytotoxicity of these NKG2A-expressing NK cells on normal T cells using EuTDA assay, where T cells served as targets. Consistently with the NK92MI experiment, co-culture with primary NK resulted in high-specific lysis of KO cells (54 ± 7.9%), whereas the specific lysis of KI cells (23 ± 5.5%) was reduced to a level comparable to the background level of WT cells (9 ± 3.9%) (Figure 8E). Lastly, we asked if the knockin strategy would also work in the bi-specific CAR-T cells. The B2M-HLA-E knockin was equally efficient in CAR-T cells (Figure 8F), and the expression of B2M-HLA-E

protected the CAR-T cells from primary NK cells as measured by the EuTDA cytotoxicity assay (WT, 2 ± 1.4%; KO, 52 ± 2.5%; and KI, 15 ± 4.0%; Figure 8G).

DISCUSSION

In this study, we expanded upon our previous research involving multi-specific CAR-T (NCT05429905) and SARS-CoV-2-specific VST cells (NCT04351659 and NCT04457726), with the aim of modifying similar clinical-grade products manufactured under GMP practices for expedient off-the-shelf adoptive cell therapy. As a proof of concept, and with the focus on the clinical translatability, we demonstrated the feasibility to KO B2M (>80%) on these multi-specific clinical-grade products by an efficient CRISPR-Cas9 based method. In addition, the process of KO could be converted into a B2M site-specific "knockin" using a newly designed g5-s2;Cas9n-AAV6 system that allows the re-expression of HLA-E, protecting B2M null cells from lysis by NK cells. The manufacturing and editing process (KO and knock in) can be performed using a single commercially available clinical instrument (e.g., CliniMACS Prodigy), paving the way for the production of off-the-shelf products with immediate availability, improved *in vivo* persistence, optimized gene-editing efficiency and safety, and reduced cost per recipient. These features are particularly attractive for CAR-T cells as all current commercial CAR-T products are autologous, with considerable product variability, manufacturing lag time, and financial burden.

All antigen-specific immunotherapies are vulnerable to immune escape via antigen loss, such as CD19-negative relapse, which commonly occurs after CD19 CAR-T therapy, or SARS-CoV-2 variants carrying RBD mutations, which led to the rapid obsolescence of U.S. Food and Drug Administration (FDA)-approved monoclonal antibodies.[17] Thus, multitargeting strategies are actively being investigated. We have previously shown excellent results with co-administration of CD19 and CD22 CAR-T.[18] Similarly, we have previously shown that COVID-19 vaccines generate broad T cell response against SMN peptides,[19] which are highly conserved across all SARS-CoV-2 variants. Although the COVID-19 pandemic has subsided, future pandemics with other virus will likely face similar challenges with antigen escape. Thus, adoptive transfer of multi-valent CAR-T and VST remains a desirable clinical goal.

Aside from antigen loss, another common mechanism of cellular therapy failure is the lack of *in vivo* persistency, which is problematic for autologous cells due to poor cell fitness and for allogeneic cells due to allo-rejection. Here, we sought to address these challenges by developing a streamlined, efficient, and genome-safe process of B2M KO and HLA-E knockin, which can be seamlessly integrated into the clinical production of allogeneic, off-the-shelf multispecific CAR-T and VST. It is well-established that B2M ablation alone is sufficient to block HLA class I surface expression,[20,21] making it an effective strategy to evade allo-rejection by $CD8^+$ T cells. Early attempts of this approach were generally unsatisfactory due to the limited editing efficiency in primary cells.[22,23] Editing clinical-grade products is even more challenging, as CAR-T and VST have been extensively manipulated *ex vivo* and may not tolerate additional cell processing. Even with CRISPR-Cas9 technology, the efficiency of B2M KO was only 50%–60% on primary T cells,[24–26] which could be increased to ∼80% with two rounds of electroporation[27] but at the cost of reducing proliferative potential to one-third. Here, we demonstrated that a high level of B2M KO (>80%) can be achieved by a single-step electroporation in the difficult-to-edit clinical-grade products, without compromising proliferative potential.

Although B2M KO prevents T cell alloreactivity, it renders the cells susceptible to NK-mediated lysis.[28,29] One strategy to mitigate NK toxicity is to re-express a B2M fused form of HLA-E on cell surface, which suppresses NK activity in the absence of endogenous B2M.[8,9] By employing paired Cas9n and HDR mediated by AAV6 delivered template, we achieved efficient "knockout by knockin" that re-expressed B2M-HLA-E in nearly 50% of the edited T cells. Of the two dominant HLA-E alleles (account for ∼100% in population), we choose HLA-E*01:03 ($HLA\text{-}E^G$) because of its higher affinity to peptide and higher level of surface expression.[30] Given that NK cells are also inhibited by killer-cell immunoglobulin-like receptors,[31] donors who are positive for all three KIR-ligand C1, C2, and Bw4 are preferable and are readily available in clinical settings to further enhance the persistence of edited CAR-T and VST.

CRIPSR-Cas9 may induce non-specific, off-target editing, leading to the development of several high-throughput methods to identify these off-target sites, including GUIDE-seq, CIRCLE-seq, SURRO-seq, and CHANGE-seq.[15,32–34] *In silico* platforms such as COSMID and Cas-OFFinder have been developed to complement or even replace these empirical methods.[35,36] Noticeably, bioinformatic pipelines with refined algorithm can predict all the off-target sites identified by empirical methods.[37] Using sequencing guided by bioinformatics prediction, our analysis revealed no significant (>1%) off-target editing in the B2M KO cells (with g5). The specificity of Cas9 editing can be significantly enhanced by the paired Cas9n approach,[11,38,39] an advantage inherent to paired nickases. This prompted us to develop a site specific B2M-HLA-E knockin using paired Cas9n with gRNAs g5 and s2. While GUIDE-seq analysis confirmed that g5 is highly specific, one major off-target site (chr22) was identified for s2. However, this off-target editing by s2 was completely eliminated by using Cas9n, rather than Cas9 nuclease, further supporting the merit of paired nickase approach. Our findings align with another recent study demonstrating that paired nickases greatly reduce off-target editing and chromosomal translocations caused by their respective nucleases.[40] Using newly designed algorithm "CAST-seq," tailored to characterize chromosomal aberrations produced by Cas9n, the authors found that paired nickases introduced chromosomal aberrations only at the on-target site, consistent with our findings on the g5-s2 pair.

T cell immunity plays a key role in the clearance of SARS-CoV-2 and resolution of COVID-19.[41,42] Patients with robust T cell immunity tend to be asymptomatic or experienced mild disease,[43] whereas those suffering from severe disease often present with T cell

dysfunction and lymphopenia.[44,45] Furthermore, immunocompromised patients may not have adequate response after vaccination, as observed in the majority of patients in our prior VST trial,[6] rendering them at risk for severe disease despite vaccination. In these contexts, adoptive transfer of SARS-CoV-2 VST from convalescent or vaccinated donors to these patients may elicit rapid and robust secondary responses, a concept previously explored for CMV, EBV, and adenovirus (ADV).[46–50] Encouraging clinical benefits was recently demonstrated in a long-term retrospective analysis.[51] A cell bank with established platform of VST production and, potentially, gene editing would effectively support viral T cell immunotherapy. Several groups, including ours,[3,52–57] have reported the production of SARS-CoV-2-specific T cells. We demonstrated that persistence of donor VST at a level detectable by clinical assay is crucial for patient outcome. Among the eight patients who had detectable donor SARS-COV-2-specific T cells following adoptive cell transfer, none progressed to severe disease or died of COVID-19. In contrast, among the other four patients without evidence of donor micro-chimerism, two died of COVID-19.[6] These observations highlight the importance of further clinical development of hypo-alloimmunogenic VST which are more durable *in vivo*, even for just a few days.[6] As demonstrated in the current study, B2M KO enables SARS-CoV-2-specific T cells to evade allo-rejection, thereby facilitating allogenic adoptive transfer. This platform can be seamlessly adapted to produce VSTs targeting other viruses. To our knowledge, this is the first report of gene editing in clinical-grade products of SARS-CoV-2-specific T cells. Emerging clinical data suggest that adoptive infusion of SARS-CoV-2-specific T cells to severe and immunocompromised individuals is safe and effective in promoting recovery.[4–6,57] Our rapid production method for hypoimmunogenic multispecific VST, which takes only 2 days for manufacturing, could be useful in future pandemics—whether caused by new variants or novel viruses.

In addition to allo-rejection, allogeneic cell therapy is also limited by graft-versus-host disease (GvHD). Knocking out the endogenous T cell receptor is technically feasible; however, it will render VST non-functional. Furthermore, endogenous TCRs have been shown to be essential for long term persistence of CAR-T.[58] Within the T cells populations, the naive and central memory T cell subsets are much more alloreactive (i.e., they react to allo-antigens, a key factor in GvHD) than effector memory T cell subsets, which have previously been exposed to other antigens (e.g., viruses, and thus becomes VSTs). To address this, our group and others have pursued naive T cell depletion instead, because the depletion process (1) does not affect the function of VST and CAR-T, (2) is technically easy, (3) does not further manipulate the genome, and (4) could be combined easily with HLA-ABC^{-} cell enrichment after B2M KO for the manufacturing of bidirectional hypo-alloimmunogenic and hypo-alloreactive cellular products. Naive T cell depletion strategy had been demonstrated successfully in CAR-T model by the removal the most alloreactive CD45RA^{+} or CD27^{+} naive T subsets from the CAR-T product.[59,60]

This study has several notable strengths and limitations. First, our experiments were on real patients' cell products, which avoid under-reporting of failed experiments or bias in using cell lines and normal T cells—which are typically easier to grow and manipulate genetically. Second, the g5 crRNA;tracrRNA and g5-s2;Cas9n-AAV6 gene-editing approaches were novel, versatile, and robust. A major limitation is that while the CAR-T and VST are hypo-alloimmunogenic, they may still be susceptible to elimination by CD4^{+} cells and macrophages. In this regard, our B2M-HLA-E design and gene-editing approach could potentially be adopted to KO CIITA and re-express CD47 in attempt to protect against rejection by CD4^{+} cells and macrophages. While our technology platform holds promise for enhancing persistence of therapeutic cells for off-the-shelf settings, further studies are needed to confirm their persistence and functionality *in vivo*.

Conclusion

In summary, we present a simple and robust platform that efficiently generates hypo-alloimmunogenic bi-specific anti-CD22/CD19 CAR-T and tri-specific anti-SMN SARS-CoV-2 T cells, which may be administered off-the-shelf with potential for better diseases control, genome-safety, immediate availability, and reduced product variability and cost.

MATERIALS AND METHODS

Ethics approval and consent to participate

The study was approved by the hospital centralized institutional review board (CIRB 2019/2866 and 2021–2063). Pan-T and NK cells were obtained as resibi-specific of apheresis product from anonymous donors contributing at the blood service group of Health Science Authority (approval 202006-08). The relevant clinical trials for bi-specific CAR-T (NCT05429905) and SARS-CoV-2-specific T cells (NCT04351659 and NCT04457726) were registered at ClinicalTrials.gov. All donors of CAR-T and SARS-CoV-2-specific T cells products were consented for research.

Manufacturing of multi-specific CAR-T cells and SARS-CoV-2 T cells

All the CAR-T and VST collected for research described herein were originally manufactured for clinical use. All donors consented to donate unused portions of their T cells for research purposes.

Bi-specific CAR-T

The CAR-T cells were produced by the Prodigy TCT System (Miltenyi). Unmobilized peripheral blood mononuclear cells were first enriched for CD4^{+} and CD8^{+} cells, which were then activated with MACS GMP T Cell TransAct (Miltenyi Biotec, Cat 130-111-160) on day 0, and were transduced by the lentiviral particles the following day (day 1). The aCD22-CD19 vector expresses a tandem CAR generated by linking anti-CD22 and anti-CD19 scFV in frame to CD8 hinge and transmembrane domain, the 4-1BB (CD137) signaling domain, and the CD3 zeta signaling domain. The expression of aCD22-CD19 CAR was detected by CD19 CAR and CD22 CAR detection reagents (cat. 130-115-965 and 130-126-727,

respectively, Miltenyi Biotec). Quality control tests (cell composition, potency, sterility, viral copy number, and replication-competent lentivirus assay) were conducted on day 5 and day 12 of the CAR-T production (Table S1). At the end of the 12-day expansion period of the bi-specific CAR-T cells in TexMACS GMP Medium supplemented with interleukin-7 (IL-7) and IL-15, the cells were harvested. The whole manufacturing process was run in a GMP-compliant Cell Therapy Facility at Health Sciences Authority or at the Stem Cell Laboratory of National University Hospital, Singapore.

Anti-SMN SARS-CoV-2-specific T

The eligibility criteria of convalescent and vaccinated donors and the overnight manufacturing process of clinical-grade SARS-CoV-2-specific T cells using automated CliniMACS Prodigy IFN-γ Cytokine Capture System (CCS) (Miltenyi Biotec) have been described previously.[3] Briefly, one unit of whole blood or leukapheresis was collected from each donor once and 1×10^9 cells were stimulated using PepTivators (Miltenyi Biotech), the overlapping peptide pools of the SARS-CoV-2 spike protein (S; cat. 130-126-700), membrane glycoprotein (M; cat. 130-126-702), and nucleocapsid phosphoprotein (N; cat. 130-126-698). Cells were labeled with the Catchmatrix reagent, which contained bispecific antibodies for CD45 and IFN-γ, and bound by MACS microbeads conjugated to IFN-γ-specific antibody. Captured SARS-CoV-2-specific T cells were analyzed by flow cytometry and cryopreserved (Table S2).

Cell preparation before and after gene-editing

Bi-specific CAR-T

Cells from the bi-specific CAR-T products were cultured in TexMACS medium (TexMACS-IL2) supplemented with 10 ng/mL human recombinant IL-2 (PeproTech, cat. 200-02) and re-activated by T Cell TransAct (Miltenyi Biotec, cat. 130-111-160) in the titer of 1:100 for 48 h before electroporation for gene editing. Cells were then recovered in the TexMACS-IL2 medium for 4 days before analysis.

SARS-CoV-2-specific T

VST were cultured in TexMACS-IL2 medium and activated by T Cell TransAct in the titer of 1:100. The cells were supplemented with fresh medium every three days for 7 to 10 days until the cell count reached $\sim 1 \times 10^6$ before electroporation.

Pan-T and NK cells

Fresh cells were isolated from the apheresis product using Pan T cell isolation kit (cat. 130-096-535) and NK cell isolation kit (cat. 130-092-657) (Miltenyi Biotec). T cells were cultured and activated following the same protocol as CAR-T. NK cells were maintained in the complete NK MACS medium (cat. 130-114-429, Miltenyi Biotec) supplemented with 100 ng/mL of IL-2.

gRNA, Cas9 RNP, electroporation, and AAV

gRNAs were designed using GPP sgRNA Designer (currently updated to CRISPick, https://portals.broadinstitute.org/gppx/crispick/public) (Table S3). The gRNAs were prepared either in form of sgRNA or in crRNA;tracrRNA duplex, were reconstituted to 2 μg/μL in duplex buffer (all from Integrated DNA Technologies, IDT). Hybridization of crRNA;tracrRNA was carried out by mixing equal molarity of crRNA and tracrRNA and heated up to 94°C for 2 min, cooled to 60°C for 1 min, and cooled to room temperature thereafter. The Cas9 RNP complex was formed by mixing 2.5 μg of Cas9 nuclease (Alt-R S.p. Cas9 Nuclease V3; IDT, cat. 1081059) with 4 μg of gRNA in 6μL of buffer R for 15 min at room temperature. The cells were washed thrice with PBS (without Ca^{2+}/Mg^{2+}), and re-suspended in the desired volume of buffer R before mixing with the Cas9 RNP. The Cas9 RNP complex was then combined with $0.1–0.2 \times 10^6$ cells in 6μL of Buffer R, and electroporated using the 10μL Neon tips with the pre-set program no. 24 of the Neon system (1,600 V, 10 ms pulse, 3 pulses) (all from Thermo Fisher Scientific, cat. MPK5000). Electroporated cells were released immediately to pre-warmed TexMACS-IL2 for recovery. For $1–2 \times 10^6$ cells, the reagents were scaled up, and the cells were electroporated using 100 μL Neon tips instead.

Same experimental setup was deployed for knockin experiment, at which a total of 4 μg of gRNAs was used for both single gRNA (4 μg, with Cas9 nuclease) or paired gRNAs (2 μg + 2 μg) to form Cas9 RNP complex (with Cas9 nuclease or nickase; Alt-R S.p. Cas9 D10A nickase, cat. 1081063, IDT). Electroporated cells ($0.1–0.2 \times 10^6$) were released immediately to 0.5 mL of pre-warmed TexMACS-IL2 in a 24-well plate and returned to the incubator for recovery; after 15 min, 10 μL of purified AAV viral particles were added to the cells and incubated further for another 4 days with medium refreshment.

Cloning of AAV template vectors and the production of AAV particles

The AAV production vectors pDGM6 (110660), pAdDeltaF6 (112867) and pAAV-GFP (32395) were obtained from Addgene. EGFP and B2M-HLA-E knockin cassettes were cloned to the backbone vector pAAV-GFP (Table S11). The knockin cassettes were flanked by 800 bps of HAs, which contained sequences identical to the upstream (5′-) and downstream (3′-) regions of the gRNA g5 cleavage sites. The P2A-EGFP sequence was cloned from pCAG-CBE4max-xCas9(3.7)-P2A-EGFP (RTW4637) (140000, Addgene). The B2M-HLA-E, which contained the first exon of B2M, a 4× G4S linker and the coding sequence of HLA-E (allele *01:03, HLA-E^G), was amplified from the clones OHu18032 (B2M) and OHu20168 (HLA-E) (both from Genscript) and the fragments were assembled at 50°C for 1 h using Gibson assembly master mix (cat. E2611S, NEB).

The pDGM6 contained the AAV6 cap genes, AAV2 rep genes, and ADV helper genes, while pAdDeltaF6 expressed ADV genes (E4, E2a, and VA). The pAAV-GFP contained inverted terminal repeat (ITR) of AAV2, allowing the production of single strand (ss) AAV. Transfection of these three vectors into the HEK293T packaging cells produced AAV particles of serotype 6 (with AAV6 cap), which are capable of infecting hematocytes, including T cells. Briefly, 4 μg each of the three vectors was mixed with 24 μL of transfection

reagents (TurboFect, cat. R0531; Thermo Fisher Scientific) and added to 7×10^6 HEK293T cells in a 10-cm dish (day 1). One day after transfection, the medium was replaced with 10 mL of DMEM + L-glutamine (without serum), and cells were incubated until day 7. On day 7, medium and cells were harvested together and cleared using 0.45 μM filter, and the AAV particles were purified using AAV purification Midi Kit following the producer's protocol (cat. 63300, Norgen Biotek). The eluted AAV was aliquoted and stored at −80°C.

Quantification of AAV particles

The titration of AAV particles was carried out using quantitative PCR as described.[61] A primer pair and probe targeting the AAV2 ITR were used to determine the number of single-strand DNA-containing AAV particle. Briefly, a 20 μL reaction containing 0.75 μL of primers (20 μM), 1μL of probe (2.5 μM), 1 μL of purified AAV elute (or standard), and 10 μL of 2× Taqman GT master mix (cat. 4371355, Thermo Fisher Scientific) was run on CFX96 Thermo cycler (Bio-Rad) under the following conditions: activation at 95°C for 3 min, 40 cycles of denaturation at 95°C for 15 s, annealing and extension at 55°C for 30 s, and plate reading. A standard curve was generated using plasmid pAAV-GFP, which, like the AAV particle, contains two copies of AAV2 ITR per molecule. The AAV elutes were estimated to contain $\sim 10 \times 10^{10}$ virus copies (VR) per μl, and $1–10 \times 10^6$ VR/cell was used for T cells infection.

T7E1 endonuclease digestion assay

The T7E1 assay was performed using the Alt-R Genome Editing Detection Kit (IDT, cat. 1075932). Genomic DNA was extracted using DNeasy Blood & Tissue Kits (QIAGEN, cat. 69504). Primers were designed to amplify the region spanning exon 1/2 of the B2M gene, as targeted by the gRNAs g1–g5, or on the regions targeted by gRNA s2 on chromosome 22 and 5, respectively (Table S3). A 20 μL PCR reaction was performed using GoTaq master mix (Promega, cat. M7122) with the following cycling parameters: 95°C for 10 min, 40 cycles of 95°C for 30 s, 55°C for 30 s, 72°C for 30 s, and final amplification of 72°C for 7 min. After PCR, 1 μL of the 10 × T7E1 reaction buffer was added to 8 μL of the PCR product, and the mixture was denatured in a thermal cycler as follows: 10 min at 95°C, cooled to 85 °C at the ramp rate of 2 °C/s, and further cooled to 25 °C at the ramp rate of 0.3 °C/s. Then, 1 μL of T7 endonuclease I (1 unit/μL) was added, and the reaction was incubated at 37°C for 1 h. The digested products were resolved on 1% agarose gel.

Purification of B2M knockout cells

The purification of B2M KO cells (HLA-ABC$^-$) were performed using magnetic bead separation. Cells were labeled with biotin-HLA-ABC antibody (cat. 130-120-571), incubated with streptavidin microbeads (cat. 130-048-101), and washed before being loaded onto the magnet-bound LD column (cat. 130-042-901). The HLA-ABC$^-$ cells were collected in the flow-through.

Flow cytometry analysis

The lymphocytes were washed once in PBS, stained with antibodies and 7AAD (1 μg/mL; cat. A1310, Thermo Fisher Scientific) for dead cell exclusion. Cells acquisition and analysis was performed by BD LSRII and FlowJo, respectively (BD Bioscience). Antibodies to use: human CD45-APC (2D1; cat. 17-9459-42) and human HLA-ABC-PE (W6/32; cat. 12-9983-42) (both from eBioscience) for B2M KO; Biotin-CD19 CAR Detection Reagent (which recombinantly expressed fusion protein consisting of the human CD19 extracellular domains; cat. 130-115-965) and Streptavidin-APC-Vio 770 (cat. 130-106-794) for CAR expression; CD45-vioblue (5B1; cat. 130-113-122), CD3-FITC (REA613; cat. 130-113-138), CD4-viogreen (REA623; cat. 130-113-230), CD8-APC-vio770 (REA734; cat. 130-110-681), CD56-PE (REA196; cat. 130-113-312), CD14-APC (REA599; cat. 130-110-520), and CD19-PE-vio770 (REA675; cat. 130-113-647) for immune composition; CD3-FITC (REA613), CD45RO-APC-vio770 (REA611; cat. 130-113-557), and CD62L-PE (REA615; cat. 130-114-151) (all from Miltenyi Biotec) for T cell subsets of SARS-CoV-2-specific T cells; CD3-FITC, HLA-ABC-PE, and HLA-E (3D12; cat. 342606, Biolegend) for knockin analysis; CD3-BV421 (UCHT1; cat. 300434, BioLegend), CD56-FITC (REA196; cat. 130-113-312, Miltenyi Biotec), HLA-ABC-PE, and HLA-E for NK92MI co-culture; CD3-APC/Cyanine7 (SK7; cat. 344818, BioLegend), CD56-PE (REA196; cat. 130-114-549), NKG2A-FITC (REA110; cat. 130-113-565), and NKG2C-APC (REA205; cat. 130-117-547) (Miltenyi Biotec) for NK cells analysis.

Mixed leukocytes reaction assay

The CAR-T or VST were used as stimulator cells, while PBMCs from anonymous donors served as responder cells. The stimulator and responder cells were resuspended in PBS and labeled by 1 μM of CellTrace Violet (cat. C34557) and 1 μM of Celltrace CFSE (cat. C34554) (both from Thermo Fisher Scientific), respectively, at 37°C for 30 min. The labeled cells were washed three times with PBS and resuspended in TexMACS-IL2. The stimulator cells were then irradiated at 30 Gy using X-ray irradiator (Radsource RS2000). Approximately 0.5×10^6 irradiated stimulator cells were combined with 1×10^6 responder cells (at 1:2 ratio) in 1 mL of TexMACS-IL2 and co-cultured for 6–7 days. The cells were then washed, stained with 7-AAD and CD3-PE (UCHT1; cat. 980008, BioLegend), and analyzed by flow cytometry. The stimulators cells were excluded based on Violet signal, and the percentage of alloreactive responder T cells was determined as the percentage of $CD3^+/CFSE^{dim}$ cells out of the total $CD3^+$ population.

DELFIA proliferation assay

Proliferation was determined by DELFIA cell proliferation kit (cat. AD0200; PerkinElmer Inc.), following manufacturer's protocol. Approximately 10,000–20,000 cells were plated per well in a 96-well plate in 200 μL of TexMACS-IL2 and incubated for five days. Cells were labeled with 1 μM BrdU for 4 h in the culture incubator before harvesting for the assay. The cells were fixed on plate, heated at 60°C for 1 h, incubated with an anti-BrdU-Europium antibody for 1 h, and then washed. Europium detection solution was then added to the well, and the Europium signal was detected using Tecan SPARK plate reader.

EuTDA cytotoxicity assay

The cytotoxic potency of CAR-T and primary NK cells was assessed using DELFIA EuTDA cytotoxicity reagent (Cat AD0116, PerkinElmer Inc.). The target cells were labeled with BATDA, a cell-permeable compound. Within viable cells, BATDA is hydrolyzed, becoming impermeable and trapped within the cells. The hydrolyzed BATDA is only released upon cell lysis, forming the fluorescent compound EuTDA in the presence of europium, generating a quantifiable fluorescent signal proportional to the extent of cell death (lysis). Briefly, about 1×10^6 of targets cells (Raji, RS4;11, and K562) were labeled with 1.25 μL of BATDA reagent in 1 mL of RPMI culture medium for 30 min at 37°C. The BATDA loaded cells were then washed three times with PBS (phosphate buffered saline), resuspended in TexMACS-IL2. The labeled cells were adjusted to 1×10^5/mL and 50 μL were added to V-bottom plate (cat. 249952; Thermo Fisher Scientific) in triplicates. The labeled cells were than mixed with 50 μL of effector (CAR-T) cells at 1×10^6/mL, 0.5×10^6/mL, 0.1×10^6/mL, or no effector, for effector-to-target (E:T) ratio of 10:1 or 5:1 and 0 (spontaneous release), respectively. For NK and T cells co-culture, the target cells (T and CAR-T cells) were labeled in the same way in TexMACS-IL2 and mixed with NK cells at E:T ratio of 2:1. Reading for maximum release was prepared by mixing 10 μL of lysis buffer and 40 μL of medium to the labeled cells. The cells were then incubated for 2 to 4 h at 37°C, after which the V-bottom plate was centrifuged for 5 min at 1,500 rpm; 20 μL of the supernatant was transferred to a microtitration plate, mixed with 200 μL of europium solution, and incubated for 15 min on orbital shaker at room temperature, protected from light. The europium signal (counts) was read using Tecan SPARK plate reader. The result was reported as percentage of specific lysis, calculated using the following formula:

$$\% \text{ Specific release} = \frac{(\text{Experimental release - Spontaneous release})}{(\text{Maximum release-Spontaneous release})} \text{ x } 100\ \% \quad \text{(Equation 1)}$$

IFN-γ detection assay

The reactivity and specificity of SARS-CoV-2-specific T cells were assessed using Rapid Cytokine Inspector Kit (cat. 130-097-343), which comprises antibodies CD3-vioblue (BW264-56), CD4-APC (VIT4), CD8-FITC (BW135/80), CD14-PerCP (TÜK4), and CD20-PerCP (LT20), along with IFN-γ-PE (cat. 130-097-600). Approximately 0.1×10^6 cells were placed in 100 μL of TexMACS (without cytokine) per well on the 96-well plate overnight. The next day, peptivator peptides were added to individual wells at 0.6 nmol/mL and incubated for 2 h. Peptivators specific for the protein S (cat. 130-126-700), N (cat. 130-126-698), and M (cat. 130-126-702) of SARS-CoV-2 were used in bulk (SMN), while peptivators for pp65 of CMV (cat. 130-093-438) or EBV (cat. 130-099-764) were used as negative control (all from Miltenyi Biotec). Brefedin A was then added to the cells at 1 μg/mL and incubated for another 4 h. The cells were then harvested for staining following the kit's protocol, and the level of intracellular IFN-γ was analyzed by flow cytometry.

CRISPR-targeted amplicon sequencing

The amplicon panel was designed using rhAmpSeq CRISPR analysis system (IDT) and produced by IDT. The panel comprised the on-target site at the first exon of B2M (site ID: On_1) and additional 14 predicted off-target loci (site ID: Off_1 to Off_14). PCR amplification of Off_14 was unsatisfactory upon sequencing and, therefore, was removed from the analysis. The amplicon library for each sample was constructed from 10 to 50 ng of genomic DNA using rhAmpSeq CRISPR library kit and was uniquely indexed. The indexed libraries were then pooled, cleaned up, and paired-end sequenced on Novaseq 6000 (Novogene; for the CAR-T samples) or HiSeq X Ten platform (BGI; for the VST samples). The indels were analyzed and visualized on the cloud-based platform (BlueBee, IDT).

PCR validation of knockin to the B2M loci

PCR was performed on the genomic DNA isolated from edited T cells using specific primers (Table S3) and GoTaq PCR master mix (cat. M7122, Promega) under the following conditions: activation at 95°C for 1 min, followed by 40 cycles of denaturation at 95°C for 30 s, annealing at 62°C for 30 s and extension at 72°C for 2 min, and with final extension at 72°C for 5 min. The amplified product was then resolved on a 1% gel agarose.

Co-culture with NK92MI cells

NK92MI (CRL-2408, ATCC) was maintained in supplemented Alpha Minimum Essential Medium (αMEM) as recommended by ATCC. For co-culture, 0.1×10^6 NK92MI and 0.1×10^6 T cells were combined in 100 μL of αMEM (supplemented with 10 ng/mL of IL-2) in a 96-well plate and incubated for 3 days before being harvested for flow cytometry analysis.

GUIDE-seq

The empirical method, which relies on the capture of integration of double-stranded oligodeoxynucleotides (dsODN) into the double-stranded break (DSBs) produced by Cas9 nuclease, was reported previously.[14,15] Briefly, blunt-ended, end-protected dsODN was prepared by annealing the two modified oligonucleotides (Table S3). The dsODN (100 pmol), along with the gRNA;Cas9 nuclease complex (with either g5 or s2), was electroporated into the activated T cells as described before. The T cells were harvested 4 days post-electroporation for genomic DNA extraction. The dsODN contains a NdeI restriction site, and the efficiency of dsODN integration was estimated by NdeI digestion of the same PCR products at the B2M site for T7E1 assay. Integration frequency of >5% was achieved in the edited samples, whereas the control (dsODN without Cas9 nuclease) showed no integration. The DNA samples were than processed by CD Genomics for GUIDE-seq analysis.

Statistical analysis

Data were reported as mean ± standard error of the mean (SEM). Statistical significance was determined using paired two tailed Student's t test.

DATA AVAILABILITY

The data that support the findings of this study are available from the corresponding author upon reasonable request.

ACKNOWLEDGMENTS

We thank our collaborators and colleagues at KK Women's and Children's Hospital (KKH), Singapore General Hospital (SGH), and Cell Therapy Facility of Health Science Authority (HSA) for their professional support. Our program, the Academic Clinical Programme-Paediatrics (PAEDS-ACP), received financial support from GOH Foundation and Children's Cancer Foundation (CCF). The SARS-CoV-2 study was funded by Singhealth Duke-NUS Academic Medicine COVID-19 Rapid Response Research Grant (AM/COV002/2020 [SRDUKAMC2002]). Both K.P.N. and M.S.-f.S. are supported by the Teo Sok Yong and Goh Cheng Liang Childhood Cancer grant. The funders had no role in study design, data collection, data analysis, data interpretation, or writing of the report. The corresponding author has full access to all the data in the study and has final responsibility for the decision to submit for publication.

AUTHOR CONTRIBUTIONS

K.P.N. and W.L. conceived and designed the experiments; K.P.N. and M.S.-f.S. conducted the research; K.P.N., M.S.-f.S. and W.L. analyzed the data; K.P.N., M.S.-f.S., and W.L. wrote the manuscript. All authors read and approved the final manuscript.

DECLARATION OF INTERESTS

W.L. is a part-time advisor to Miltenyi Biomedicine.

SUPPLEMENTAL INFORMATION

Supplemental information can be found online at https://doi.org/10.1016/j.omtm.2025.101462.

REFERENCES

1. Cappell, K.M., and Kochenderfer, J.N. (2023). Long-term outcomes following CAR T cell therapy: what we know so far. Nat. Rev. Clin. Oncol. *20*, 359–371. https://doi.org/10.1038/s41571-023-00754-1.

2. Mahadeo, K.M., Baiocchi, R., Beitinjaneh, A., Chaganti, S., Choquet, S., Dierickx, D., Dinavahi, R., Duan, X., Gamelin, L., Ghobadi, A., et al. (2024). Tabelecleucel for allogeneic haematopoietic stem-cell or solid organ transplant recipients with Epstein-Barr virus-positive post-transplant lymphoproliferative disease after failure of rituximab or rituximab and chemotherapy (ALLELE): a phase 3, multicentre, open-label trial. Lancet Oncol. *25*, 376–387. https://doi.org/10.1016/S1470-2045(23)00649-6.

3. Leung, W., Soh, T.G., Linn, Y.C., Low, J.G.H., Loh, J., Chan, M., Chng, W.J., Koh, L.P., Poon, M.L.M., Ng, K.P., et al. (2020). Rapid production of clinical-grade SARS-CoV-2 specific T cells. Adv. Cell Gene Ther. *3*, e101. https://doi.org/10.1002/acg2.101.

4. Haidar, G., Jacobs, J.L., Kramer, K.H., Naqvi, A., Heaps, A., Parikh, U., McCormick, K.D., Sobolewski, M.D., Agha, M., Bogdanovich, T., et al. (2023). Therapy With Allogeneic Severe Acute Respiratory Syndrome Coronavirus-2-Specific T Cells for Persistent Coronavirus Disease 2019 in Immunocompromised Patients. Clin. Infect. Dis. *77*, 696–702. https://doi.org/10.1093/cid/ciad233.

5. Papadopoulou, A., Karavalakis, G., Papadopoulou, E., Xochelli, A., Bousiou, Z., Vogiatzoglou, A., Papayanni, P.G., Georgakopoulou, A., Giannaki, M., Stavridou, F., et al. (2023). SARS-CoV-2-specific T cell therapy for severe COVID-19: a randomized phase 1/2 trial. Nat. Med. *29*, 2019–2029. https://doi.org/10.1038/s41591-023-02480-8.

6. Seng, M.S.F., Ng, K.P., Soh, T.G., Tan, T.T., Chan, M., Maiwald, M., Tan, L.K., Linn, Y.C., and Leung, W. (2024). A phase I/II study of adoptive SARS-CoV-2-specific T cells in immunocompromised hosts with or at risk of severe COVID-19 infection. Cytotherapy *26*, 1170–1178. https://doi.org/10.1016/j.jcyt.2024.05.014.

7. Hendel, A., Bak, R.O., Clark, J.T., Kennedy, A.B., Ryan, D.E., Roy, S., Steinfeld, I., Lunstad, B.D., Kaiser, R.J., Wilkens, A.B., et al. (2015). Chemically modified guide RNAs enhance CRISPR-Cas genome editing in human primary cells. Nat. Biotechnol. *33*, 985–989. https://doi.org/10.1038/nbt.3290.

8. Gornalusse, G.G., Hirata, R.K., Funk, S.E., Riolobos, L., Lopes, V.S., Manske, G., Prunkard, D., Colunga, A.G., Hanafi, L.A., Clegg, D.O., et al. (2017). HLA-E-expressing pluripotent stem cells escape allogeneic responses and lysis by NK cells. Nat. Biotechnol. *35*, 765–772. https://doi.org/10.1038/nbt.3860.

9. Guo, Y., Xu, B., Wu, Z., Bo, J., Tong, C., Chen, D., Wang, J., Wang, H., Wang, Y., and Han, W. (2021). Mutant B2M-HLA-E and B2M-HLA-G fusion proteins protects universal chimeric antigen receptor-modified T cells from allogeneic NK cell-mediated lysis. Eur. J. Immunol. *51*, 2513–2521. https://doi.org/10.1002/eji.202049107.

10. Jo, S., Das, S., Williams, A., Chretien, A.S., Pagliardini, T., Le Roy, A., Fernandez, J.P., Le Clerre, D., Jahangiri, B., Chion-Sotinel, I., et al. (2022). Endowing universal CAR T-cell with immune-evasive properties using TALEN-gene editing. Nat. Commun. *13*, 3453. https://doi.org/10.1038/s41467-022-30896-2.

11. Ran, F.A., Hsu, P.D., Lin, C.Y., Gootenberg, J.S., Konermann, S., Trevino, A.E., Scott, D.A., Inoue, A., Matoba, S., Zhang, Y., and Zhang, F. (2013). Double nicking by RNA-guided CRISPR Cas9 for enhanced genome editing specificity. Cell *154*, 1380–1389. https://doi.org/10.1016/j.cell.2013.08.021.

12. Bothmer, A., Phadke, T., Barrera, L.A., Margulies, C.M., Lee, C.S., Buquicchio, F., Moss, S., Abdulkerim, H.S., Selleck, W., Jayaram, H., et al. (2017). Characterization of the interplay between DNA repair and CRISPR/Cas9-induced DNA lesions at an endogenous locus. Nat. Commun. *8*, 13905. https://doi.org/10.1038/ncomms13905.

13. Tran, N.T., Danner, E., Li, X., Graf, R., Lebedin, M., de la Rosa, K., Kühn, R., Rajewsky, K., and Chu, V.T. (2022). Precise CRISPR-Cas-mediated gene repair with minimal off-target and unintended on-target mutations in human hematopoietic stem cells. Sci. Adv. *8*, eabm9106. https://doi.org/10.1126/sciadv.abm9106.

14. Malinin, N.L., Lee, G., Lazzarotto, C.R., Li, Y., Zheng, Z., Nguyen, N.T., Liebers, M., Topkar, V.V., Iafrate, A.J., Le, L.P., et al. (2021). Defining genome-wide CRISPR-Cas genome-editing nuclease activity with GUIDE-seq. Nat. Protoc. *16*, 5592–5615. https://doi.org/10.1038/s41596-021-00626-x.

15. Tsai, S.Q., Zheng, Z., Nguyen, N.T., Liebers, M., Topkar, V.V., Thapar, V., Wyvekens, N., Khayter, C., Iafrate, A.J., Le, L.P., et al. (2015). GUIDE-seq enables genome-wide profiling of off-target cleavage by CRISPR-Cas nucleases. Nat. Biotechnol. *33*, 187–197. https://doi.org/10.1038/nbt.3117.

16. Kamiya, T., Seow, S.V., Wong, D., Robinson, M., and Campana, D. (2019). Blocking expression of inhibitory receptor NKG2A overcomes tumor resistance to NK cells. J. Clin. Investig. *129*, 2094–2106. https://doi.org/10.1172/JCI123955.

17. Iacobucci, G. (2023). Covid-19: FDA removes US authorisation for antibody drug Evusheld. BMJ *380*, 264. https://doi.org/10.1136/bmj.p264.

18. Wang, T., Tang, Y., Cai, J., Wan, X., Hu, S., Lu, X., Xie, Z., Qiao, X., Jiang, H., Shao, J., et al. (2023). Coadministration of CD19- and CD22-Directed Chimeric Antigen Receptor T-Cell Therapy in Childhood B-Cell Acute Lymphoblastic Leukemia: A Single-Arm, Multicenter, Phase II Trial. J. Clin. Oncol. *41*, 1670–1683. https://doi.org/10.1200/JCO.22.01214.

19. Rosa Duque, J.S., Wang, X., Leung, D., Cheng, S.M.S., Cohen, C.A., Mu, X., Hachim, A., Zhang, Y., Chan, S.M., Chaothai, S., et al. (2022). Immunogenicity and reactogenicity of SARS-CoV-2 vaccines BNT162b2 and CoronaVac in healthy adolescents. Nat. Commun. *13*, 3700. https://doi.org/10.1038/s41467-022-31485-z.

20. Riolobos, L., Hirata, R.K., Turtle, C.J., Wang, P.R., Gornalusse, G.G., Zavajlevski, M., Riddell, S.R., and Russell, D.W. (2013). HLA engineering of human pluripotent stem cells. Mol. Ther. *21*, 1232–1241. https://doi.org/10.1038/mt.2013.59.

21. Torikai, H., Reik, A., Soldner, F., Warren, E.H., Yuen, C., Zhou, Y., Crossland, D.L., Huls, H., Littman, N., Zhang, Z., et al. (2013). Toward eliminating HLA class I expression to generate universal cells from allogeneic donors. Blood *122*, 1341–1349. https://doi.org/10.1182/blood-2013-03-478255.

22. Lu, P., Chen, J., He, L., Ren, J., Chen, H., Rao, L., Zhuang, Q., Li, H., Li, L., Bao, L., et al. (2013). Generating hypoimmunogenic human embryonic stem cells by the disruption of beta 2-microglobulin. Stem Cell Rev. Rep. *9*, 806–813. https://doi.org/10.1007/s12015-013-9457-0.

23. Wang, D., Quan, Y., Yan, Q., Morales, J.E., and Wetsel, R.A. (2015). Targeted Disruption of the beta2-Microglobulin Gene Minimizes the Immunogenicity of Human Embryonic Stem Cells. Stem Cells Transl. Med. *4*, 1234–1245. https://doi.org/10.5966/sctm.2015-0049.

24. Liu, X., Zhang, Y., Cheng, C., Cheng, A.W., Zhang, X., Li, N., Xia, C., Wei, X., Liu, X., and Wang, H. (2017). CRISPR-Cas9-mediated multiplex gene editing in CAR-T cells. Cell Res. *27*, 154–157. https://doi.org/10.1038/cr.2016.142.

25. Kagoya, Y., Guo, T., Yeung, B., Saso, K., Anczurowski, M., Wang, C.H., Murata, K., Sugata, K., Saijo, H., Matsunaga, Y., et al. (2020). Genetic Ablation of HLA Class I, Class II, and the T-cell Receptor Enables Allogeneic T Cells to Be Used for Adoptive T-cell Therapy. Cancer Immunol. Res. *8*, 926–936. https://doi.org/10.1158/2326-6066.CIR-18-0508.

26. Hamilton, J.R., Tsuchida, C.A., Nguyen, D.N., Shy, B.R., McGarrigle, E.R., Sandoval Espinoza, C.R., Carr, D., Blaeschke, F., Marson, A., and Doudna, J.A. (2021). Targeted delivery of CRISPR-Cas9 and transgenes enables complex immune cell engineering. Cell Rep. *35*, 109207. https://doi.org/10.1016/j.celrep.2021.109207.

27. Ren, J., Liu, X., Fang, C., Jiang, S., June, C.H., and Zhao, Y. (2017). Multiplex Genome Editing to Generate Universal CAR T Cells Resistant to PD1 Inhibition. Clin. Cancer Res. *23*, 2255–2266. https://doi.org/10.1158/1078-0432.CCR-16-1300.

28. Liao, N.S., Bix, M., Zijlstra, M., Jaenisch, R., and Raulet, D. (1991). MHC class I deficiency: susceptibility to natural killer (NK) cells and impaired NK activity. Science *253*, 199–202. https://doi.org/10.1126/science.1853205.

29. Storkus, W.J., Howell, D.N., Salter, R.D., Dawson, J.R., and Cresswell, P. (1987). NK susceptibility varies inversely with target cell class I HLA antigen expression. J. Immunol. *138*, 1657–1659.

30. Kanevskiy, L., Erokhina, S., Kobyzeva, P., Streltsova, M., Sapozhnikov, A., and Kovalenko, E. (2019). Dimorphism of HLA-E and its Disease Association. Int. J. Mol. Sci. *20*, 5496. https://doi.org/10.3390/ijms20215496.

31. Leung, W. (2014). Infusions of allogeneic natural killer cells as cancer therapy. Clin. Cancer Res. *20*, 3390–3400. https://doi.org/10.1158/1078-0432.CCR-13-1766.

32. Tsai, S.Q., Nguyen, N.T., Malagon-Lopez, J., Topkar, V.V., Aryee, M.J., and Joung, J. K. (2017). CIRCLE-seq: a highly sensitive in vitro screen for genome-wide CRISPR-Cas9 nuclease off-targets. Nat. Methods *14*, 607–614. https://doi.org/10.1038/nmeth.4278.

33. Pan, X., Qu, K., Yuan, H., Xiang, X., Anthon, C., Pashkova, L., Liang, X., Han, P., Corsi, G.I., Xu, F., et al. (2022). Massively targeted evaluation of therapeutic CRISPR off-targets in cells. Nat. Commun. *13*, 4049. https://doi.org/10.1038/s41467-022-31543-6.

34. Lazzarotto, C.R., Malinin, N.L., Li, Y., Zhang, R., Yang, Y., Lee, G., Cowley, E., He, Y., Lan, X., Jividen, K., et al. (2020). CHANGE-seq reveals genetic and epigenetic effects on CRISPR-Cas9 genome-wide activity. Nat. Biotechnol. *38*, 1317–1327. https://doi.org/10.1038/s41587-020-0555-7.

35. Bae, S., Park, J., and Kim, J.S. (2014). Cas-OFFinder: a fast and versatile algorithm that searches for potential off-target sites of Cas9 RNA-guided endonucleases. Bioinformatics *30*, 1473–1475. https://doi.org/10.1093/bioinformatics/btu048.

36. Cradick, T.J., Qiu, P., Lee, C.M., Fine, E.J., and Bao, G. (2014). COSMID: A Web-based Tool for Identifying and Validating CRISPR/Cas Off-target Sites. Mol. Ther. Nucleic Acids *3*, e214. https://doi.org/10.1038/mtna.2014.64.

37. Cromer, M.K., Majeti, K.R., Rettig, G.R., Murugan, K., Kurgan, G.L., Bode, N.M., Hampton, J.P., Vakulskas, C.A., Behlke, M.A., and Porteus, M.H. (2023). Comparative analysis of CRISPR off-target discovery tools following ex vivo editing of CD34(+) hematopoietic stem and progenitor cells. Mol. Ther. *31*, 1074–1087. https://doi.org/10.1016/j.ymthe.2023.02.011.

38. Gopalappa, R., Suresh, B., Ramakrishna, S., and Kim, H.H. (2018). Paired D10A Cas9 nickases are sometimes more efficient than individual nucleases for gene disruption. Nucleic Acids Res. *46*, e71. https://doi.org/10.1093/nar/gky222.

39. Mali, P., Aach, J., Stranges, P.B., Esvelt, K.M., Moosburner, M., Kosuri, S., Yang, L., and Church, G.M. (2013). CAS9 transcriptional activators for target specificity screening and paired nickases for cooperative genome engineering. Nat. Biotechnol. *31*, 833–838. https://doi.org/10.1038/nbt.2675.

40. Klermund, J., Rhiel, M., Kocher, T., Chmielewski, K.O., Bischof, J., Andrieux, G., El Gaz, M., Hainzl, S., Boerries, M., Cornu, T.I., et al. (2024). On- and off-target effects of paired CRISPR-Cas nickase in primary human cells. Mol. Ther. *32*, 1298–1310. https://doi.org/10.1016/j.ymthe.2024.03.006.

41. Zheng, M., Gao, Y., Wang, G., Song, G., Liu, S., Sun, D., Xu, Y., and Tian, Z. (2020). Functional exhaustion of antiviral lymphocytes in COVID-19 patients. Cell. Mol. Immunol. *17*, 533–535. https://doi.org/10.1038/s41423-020-0402-2.

42. Tan, A.T., Linster, M., Tan, C.W., Le Bert, N., Chia, W.N., Kunasegaran, K., Zhuang, Y., Tham, C.Y.L., Chia, A., Smith, G.J.D., et al. (2021). Early induction of functional SARS-CoV-2-specific T cells associates with rapid viral clearance and mild disease in COVID-19 patients. Cell Rep. *34*, 108728. https://doi.org/10.1016/j.celrep.2021.108728.

43. Sekine, T., Perez-Potti, A., Rivera-Ballesteros, O., Strålin, K., Gorin, J.B., Olsson, A., Llewellyn-Lacey, S., Kamal, H., Bogdanovic, G., Muschiol, S., et al. (2020). Robust T Cell Immunity in Convalescent Individuals with Asymptomatic or Mild COVID-19. Cell *183*, 158–168.e14. https://doi.org/10.1016/j.cell.2020.08.017.

44. Zheng, H.Y., Zhang, M., Yang, C.X., Zhang, N., Wang, X.C., Yang, X.P., Dong, X.Q., and Zheng, Y.T. (2020). Elevated exhaustion levels and reduced functional diversity of T cells in peripheral blood may predict severe progression in COVID-19 patients. Cell. Mol. Immunol. *17*, 541–543. https://doi.org/10.1038/s41423-020-0401-3.

45. Schub, D., Klemis, V., Schneitler, S., Mihm, J., Lepper, P.M., Wilkens, H., Bals, R., Eichler, H., Gärtner, B.C., Becker, S.L., et al. (2020). High levels of SARS-CoV-2-specific T cells with restricted functionality in severe courses of COVID-19. JCI Insight *5*, e142167. https://doi.org/10.1172/jci.insight.142167.

46. Feuchtinger, T., Opherk, K., Bethge, W.A., Topp, M.S., Schuster, F.R., Weissinger, E. M., Mohty, M., Or, R., Maschan, M., Schumm, M., et al. (2010). Adoptive transfer of pp65-specific T cells for the treatment of chemorefractory cytomegalovirus disease or reactivation after haploidentical and matched unrelated stem cell transplantation. Blood *116*, 4360–4367. https://doi.org/10.1182/blood-2010-01-262089.

47. Feuchtinger, T., Matthes-Martin, S., Richard, C., Lion, T., Fuhrer, M., Hamprecht, K., Handgretinger, R., Peters, C., Schuster, F.R., Beck, R., et al. (2006). Safe adoptive transfer of virus-specific T-cell immunity for the treatment of systemic adenovirus infection after allogeneic stem cell transplantation. Br. J. Haematol. *134*, 64–76. https://doi.org/10.1111/j.1365-2141.2006.06108.x.

48. Kazi, S., Mathur, A., Wilkie, G., Cheal, K., Battle, R., McGowan, N., Fraser, N., Hargreaves, E., Turner, D., Campbell, J.D.M., et al. (2019). Long-term follow up after third-party viral-specific cytotoxic lymphocytes for immunosuppression- and Epstein-Barr virus-associated lymphoproliferative disease. Haematologica *104*, e356–e359. https://doi.org/10.3324/haematol.2018.207548.

49. Barrett, A.J., Prockop, S., and Bollard, C.M. (2018). Virus-Specific T Cells: Broadening Applicability. Biol. Blood Marrow Transplant. *24*, 13–18. https://doi.org/10.1016/j.bbmt.2017.10.004.

50. Papadopoulou, A., Gerdemann, U., Katari, U.L., Tzannou, I., Liu, H., Martinez, C., Leung, K., Carrum, G., Gee, A.P., Vera, J.F., et al. (2014). Activity of broad-spectrum T cells as treatment for AdV, EBV, CMV, BKV, and HHV6 infections after HSCT. Sci. Transl. Med. *6*, 242ra83. https://doi.org/10.1126/scitranslmed.3008825.

51. Neller, M.A., Ambalathingal, G.R., Hamad, N., Sasadeusz, J., Pearson, R., Holmes-Liew, C.L., Singhal, D., Tunbridge, M., Ng, W.Y., Sharplin, K., et al. (2024). Compassionate access to virus-specific T cells for adoptive immunotherapy over 15 years. Nat. Commun. *15*, 10339. https://doi.org/10.1038/s41467-024-54595-2.

52. Cooper, R.S., Fraser, A.R., Smith, L., Burgoyne, P., Imlach, S.N., Jarvis, L.M., Turner, D.M., Zahra, S., Turner, M.L., and Campbell, J.D.M. (2020). Rapid GMP-Compliant Expansion of SARS-CoV-2-Specific T Cells From Convalescent Donors for Use as an Allogeneic Cell Therapy for COVID-19. Front. Immunol. *11*, 598402. https://doi.org/10.3389/fimmu.2020.598402.

53. Ferreras, C., Pascual-Miguel, B., Mestre-Durán, C., Navarro-Zapata, A., Clares-Villa, L., Martín-Cortázar, C., De Paz, R., Marcos, A., Vicario, J.L., Balas, A., et al. (2021). SARS-CoV-2-Specific Memory T Lymphocytes From COVID-19 Convalescent Donors: Identification, Biobanking, and Large-Scale Production for Adoptive Cell Therapy. Front. Cell Dev. Biol. *9*, 620730. https://doi.org/10.3389/fcell.2021.620730.

54. Keller, M.D., Harris, K.M., Jensen-Wachspress, M.A., Kankate, V.V., Lang, H., Lazarski, C.A., Durkee-Shock, J., Lee, P.H., Chaudhry, K., Webber, K., et al. (2020). SARS-CoV-2-specific T cells are rapidly expanded for therapeutic use and target conserved regions of the membrane protein. Blood *136*, 2905–2917. https://doi.org/10.1182/blood.2020008488.

55. Kim, N., Lee, J.M., Oh, E.J., Jekarl, D.W., Lee, D.G., Im, K.I., and Cho, S.G. (2021). Off-the-Shelf Partial HLA Matching SARS-CoV-2 Antigen Specific T Cell Therapy: A New Possibility for COVID-19 Treatment. Front. Immunol. *12*, 751869. https://doi.org/10.3389/fimmu.2021.751869.

56. Panikkar, A., Lineburg, K.E., Raju, J., Chew, K.Y., Ambalathingal, G.R., Rehan, S., Swaminathan, S., Crooks, P., Le Texier, L., Beagley, L., et al. (2022). SARS-CoV-2-specific T cells generated for adoptive immunotherapy are capable of recognizing multiple SARS-CoV-2 variants. PLoS Pathog. *18*, e1010339. https://doi.org/10.1371/journal.ppat.1010339.

57. Vasileiou, S., Hill, L., Kuvalekar, M., Workineh, A.G., Watanabe, A., Velazquez, Y., Lulla, S., Mooney, K., Lapteva, N., Grilley, B.J., et al. (2023). Allogeneic, off-the-shelf, SARS-CoV-2-specific T cells (ALVR109) for the treatment of COVID-19 in high-risk patients. Haematologica *108*, 1840–1850. https://doi.org/10.3324/haematol.2022.281946.

58. Stenger, D., Stief, T.A., Kaeuferle, T., Willier, S., Rataj, F., Schober, K., Vick, B., Lotfi, R., Wagner, B., Grünewald, T.G.P., et al. (2020). Endogenous TCR promotes in vivo persistence of CD19-CAR-T cells compared to a CRISPR/Cas9-mediated TCR knockout CAR. Blood *136*, 1407–1418. https://doi.org/10.1182/blood.2020005185.

59. Talleur, A.C., Métais, J., Li, Y., Throm, R.E., Tillman, H., Rooney, B., Moustaki, A., and Leung, W. (2019). Allogeneic CD 27-depleted cells in adoptive cell therapy. Adv. Cell Gene Ther. *2*, e45. https://doi.org/10.1002/acg2.45.

60. Chan, W.K., Suwannasaen, D., Throm, R.E., Li, Y., Eldridge, P.W., Houston, J., Gray, J.T., Pui, C.H., and Leung, W. (2015). Chimeric antigen receptor-redirected CD45RA-negative T cells have potent antileukemia and pathogen memory response without graft-versus-host activity. Leukemia *29*, 387–395. https://doi.org/10.1038/leu.2014.174.

61. Lamsfus-Calle, A., Daniel-Moreno, A., Ureña-Bailén, G., Rottenberger, J., Raju, J., Epting, T., Marciano, S., Heumos, L., Baskaran, P., S Antony, J., et al. (2021). Universal Gene Correction Approaches for beta-hemoglobinopathies Using CRISPR-Cas9 and Adeno-Associated Virus Serotype 6 Donor Templates. CRISPR J. *4*, 207–222. https://doi.org/10.1089/crispr.2020.0141.